Ann. Physik 5 (1996) 652–695

Annalen
der Physik

Transport properties of quantum dots

Dietmar Weinmann*, Wolfgang Häusler, and Bernhard Kramer

Universität Hamburg, I. Institut für Theoretische Physik, Jungiusstr. 9, D-20355 Hamburg, Germany

Received 19 April 1996, revised version 5 July 1996, accepted 9 July 1996

Abstract. Linear and nonlinear transport through a quantum dot that is weakly coupled to ideal quantum leads is investigated in the parameter regime where charging and geometrical quantization effects coexist. The exact eigenstates and spins of a finite number of correlated electrons confined within the dot are combined with a rate equation. The current is calculated in the regime of sequential tunneling. The analytic solution for an Anderson impurity is given. The phenomenological charging model is compared with the quantum mechanical model for interacting electrons. The current-voltage characteristics show Coulomb blockade. The excited states lead to additional fine-structure in the current voltage characteristics. Asymmetry in the coupling between the quantum dot and the leads causes asymmetry in the conductance peaks which is reversed with the bias voltage. The spin selection rules can cause a 'spin blockade' which decreases the current when certain excited states become involved in the transport. In two-dimensional dots, peaks in the linear conductance can be suppressed at low temperatures, when the total spins of the corresponding ground states differ by more than 1/2. In a magnetic field, an electron number parity effect due to the different spins of the many-electron ground states is predicted in addition to the vanishing of the spin blockade effect. All of the predicted features are consistent with recent experiments.

Keywords: Quantum dot transport; Electron-electron interaction; Coulomb blockade.

1 Introduction

Due to the considerable progresses in nanostructure fabrication and cryo-technology the physics of mesoscopic systems has attracted much attention during the last ten years. Systems with typical geometrical diameters that are small as compared to the phase coherence length L_φ show a great variety of new quantum phenomena [1, 2].

On the basis of these effects, new electronic devices were proposed. Most promising for future applications in electronic data processing and communication are the single electron tunneling (SET) transistors [3, 4]. In SET-devices, a controlled transfer of electrons – one by one – can be achieved [5] by applying AC-voltages [6–9]. This could also open the way to a new current standard based on counting the electrons that pass the device per unit of time [10–12].

Thus, transport properties of mesoscopic systems are highly interesting in view of possible future applications. The main problem is the very low temperature needed to

* On leave from Universität Stuttgart, II. Institut f. Theoret. Physik, Pfaffenwaldring 57, 70550 Stuttgart, Germany; present address: CEA/DSM/DRECAM/SPEC, CEN Saclay, 91191 Gif-sur-Yvette, France.

operate such devices. However, charging effects have recently been observed in ultrasmall systems even at room temperature [13].

Investigating mesoscopic systems is also of great fundamental importance. They allow to study the transition from quantum to classical behavior since typical geometrical dimensions and numbers of degrees of freedom lie in the intermediate regime between the quantum world of the atoms, and the macroscopic systems of every days life. Furthermore, the comparatively small number of electrons in well-controllable small systems allows to investigate few interacting particles experimentally as well as theoretically, thus contributing to increase the general understanding of many-particle physics [15]. It is now possible to create "artificial atoms" [4] by confining electrons within potential wells – so-called quantum dots – and to tune externally electron number and geometrical dimensions by applying gate-voltages.

When only a few electrons are confined in very small dots, Coulomb interaction influences strongly the excitation spectrum. By investigating arrays of ultrasmall dots with infrared absorption spectroscopy [17–19], electron numbers as low as only one or two can be studied. In these experiments, the confining potential is almost inevitably parabolic and the radiation couples only to the center of mass degree of freedom of the electrons. Then, the effects of correlations are very difficult to observe, according to Kohn's theorem [21].

Capacitance spectroscopy [22] has also been used to investigate the spectra of ultrasmall single quantum dots which contain very small numbers of electrons. Here, only equilibrium properties play a role. No information about excited states is obtained.

In contrast, nonlinear transport experiments on single quantum dots yield in principle the complete spectrum of the excited states [23, 24]. When the quantum dot and the leads, which connect to the macroscopic world, are only weakly coupled, the transport will be dominated by the quantum properties of the electrons in the isolated dot. If the latter is very small, the charging energy E_C, that is needed to add an electron, can exceed considerably the thermal energy $k_B T$. Then, the linear current is suppressed. This is the Coulomb blockade effect [10]. For small voltages, and at low temperatures, no current flows if for the chemical potentials μ_L and μ_R of the reservoirs on the left and on the right hand side of the dot, respectively, $\mu_L \approx \mu_R \neq E_0(n) - E_0(n-1)$. Here, $E_0(n)$ is the ground state energy of n electrons.

On the other hand, if $\mu_L \approx \mu_R = E_0(n) - E_0(n-1)$, the number of electrons inside the dot can oscillate between n and $n-1$ (SET oscillations), the conductance is finite. The resulting periodic oscillations of the conductance as a function of external parameters like gate voltage (change in electron density) or magnetic field (change in energy spectrum) [3, 25–27] are well established consequences of the charging energy. They can be observed when $k_B T \ll E_C$, such that thermal smearing is suppressed, and if the coupling to the leads (tunnel-resistance R_T) is sufficiently weak, $R_T \gg h/e^2$, in order to avoid quantum smearing. This guarantees that the electron number n is a good quantum number on a sufficiently long timescale. The heights and the widths of the peaks depend on the temperature and the coupling to the leads [28].

In GaAs/GaAlAs heterostructures, two-dimensional electron gas of high mobility is generated at the interface by properly doping the different materials. Depletion by applying negative voltages to suitably shaped metallic gates on top of the sample, which are separated from the electron gas by insulating layers, leads to ultra-small electron islands – 'quantum dots' – that are weakly connected by tunnel barriers to

'leads' [29]. Even the height of the barriers can be tuned by changing the gate voltages.

The electron density in these systems is considerably lower than in metals. The excitation energies for a fixed number of particles can exceed considerably the thermal energy at millikelvin-temperatures which are available in ^{3}He-^{4}He dilution refrigerators. At bias voltages V larger than the differences between the quasi-discrete excitation energies of the electron island, additional steps in the current as a function of the bias voltage occur [23, 29–36]. They are due to transitions between the excited states of n and $n+1$ electrons and cannot be fully understood by using the semi-classical charging model. Kohn's theorem [21] is circumvented in these experiments and information about the spectrum of the excited states of the interacting electrons in the quantum dot can be obtained via non-linear transport [30, 31].

It is the main purpose of the present paper to describe extensively the transport properties in this regime. We combine the results of exact quantum mechanical calculations of the energy spectra of a few – up to four – electrons, and the corresponding eigenstates with a rate equation and calculate the non-linear current-voltage characteristic in the region of sequential tunneling. In addition to recovering the transport phenomena related to the usual Coulomb blockade mechanism, we predict a number of additional striking non-linear transport effects that are related to quantum mechanical selection rules. The spin selection rule is only one example. Additional features are related to the spatial properties of the many particle states. All of these are genuine quantum effects and are discussed extensively in the following sections.

In the semi-classical model of quantum dot transport the quantum mechanical correlation effects are neglected. Here, the current increases with increasing bias voltage V. In contrast – as we will extensively discuss below – when the quantum effects are fully taken into account, the current does not necessarily increase when, by increasing V, the number of transitions between n and $n-1$ electron states increases. Especially spin selection rules can suppress very effectively certain transitions and thus *reduce* the current. This happens, for instance, if the electrons in the dot are spin-polarized, and the total spin adopts its maximum value, $S = n/2$. Then, the electron number can only be decreased if simultaneously the total spin is reduced [24]. Regions of negative differential conductance may be caused by this 'spin blockade'. It is a consequence of the existence of excited states with different total spins [24, 37, 38, 40, 41]. Such regions have been observed in recent experiments [23, 31].

Negative differential conductances have also been found in the transport through a two-dimensional (2D) dot with parabolic confinement in the fractional quantum Hall (FQHE) regime without spin [42]. Here, the effect is assumed to originate in excited states for which the coupling to the leads is weaker than for the ground state.

The transport properties were also investigated in the presence of a magnetic field parallel to the current [23, 43]. The results of our calculations are fully consistent with these experiments.

The paper is organized as follows. In Sections 2 and 3 we describe the model and the method of calculation, respectively. Section 4 contains a tutorial example – the Anderson impurity. In the Section 5 the conventional charging model is discussed to some extent. In the Section 6 a 1D quantum dot is treated fully quantum mechanically. The current-voltage characteristic is calculated, and the various additional blockade effects are discussed. A full account of the predicted features in the non-linear transport spectra is provided in this section. In the Section 7, the influence of a magnetic field on the transport spectra is investigated. In Section 8, the results for a

2D quantum are presented and discussed. New effects related to quantum selection rules are here predicted. A short summary of the new quantum transport effects is given in Section 9 together with a discussion of the possibilities of experimental verification.

2 The model

2.1 The tunneling Hamiltonian

For the theoretical treatment of systems in which different regions of a sample are only very weakly coupled via tunneling barriers (Fig. 1), the so-called tunneling Hamiltonian was proposed [44]. This approach has serious problems [45] because it is not possible to deduce the Hamiltonian unambiguously from first principles using a model for the barrier potential. Justification is only possible in lowest order of the tunneling matrix elements.

However, the tunneling Hamiltonian is very successful for describing weak links. It allows to treat the tunneling as a weak perturbation to the decoupled system which is exactly the limit where the Hamiltonian can be justified.

As a model for an electronic island weakly connected to quantum wires on the left and on the right (Figs. 1 and 2), we consider the double barrier tunneling Hamiltonian

$$H = H_{\mathrm{L}} + H_{\mathrm{R}} + H_{\mathrm{D}} + H_{\mathrm{L}}^{\mathrm{T}} + H_{\mathrm{R}}^{\mathrm{T}} + H_{\mathrm{Ph}} + H_{\mathrm{ep}}\,. \tag{1}$$

Here,

$$H_{\mathrm{L/R}} = \sum_{k,\sigma} \varepsilon_k^{\mathrm{L/R}} c_{\mathrm{L/R},k,\sigma}^{+} c_{\mathrm{L/R},k,\sigma} \tag{2}$$

describe free electrons in the left/right lead. The operators $c_{\mathrm{L/R},k,\sigma}^{+}$ and $c_{\mathrm{L/R},k,\sigma}$ create and annihilate electrons with wave vector k and spin σ in the left/right lead, respec-

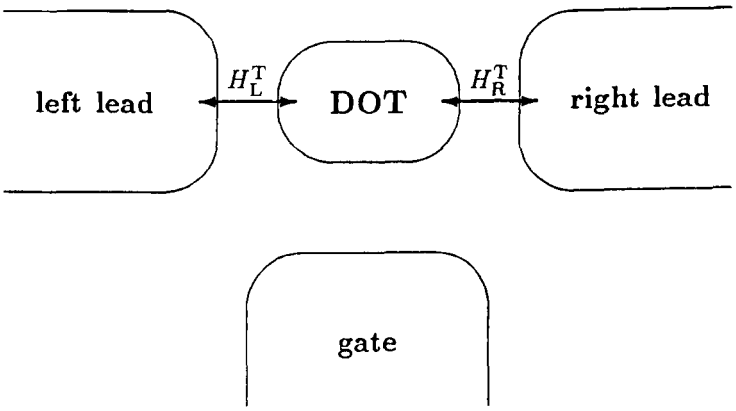

Fig. 1 Schematic picture of the quantum dot, the left/right and the gate electrodes. The tunneling junctions are modeled by the terms $H_{\mathrm{L/R}}^{\mathrm{T}}$.

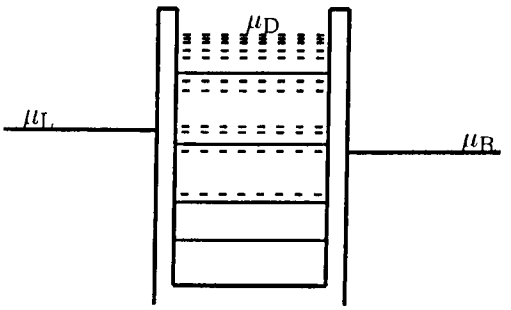

Fig. 2 The double barrier potential model. There are electrons at both sides of the structure up to the chemical potentials $\mu_{L/R}$. In the dot, energy differences between discrete states corresponding to subsequent electron numbers are indicated. Solid lines stand for ground state to ground state energy differences while dashed lines involve excited many-electron levels.

tively. The leads are assumed to be connected to very large reservoirs at temperature T. We describe the occupation of their states by the Fermi-Dirac distributions $f_{L/R}(\varepsilon) = (\exp[\beta(\varepsilon - \mu_{L/R})] + 1)^{-1}$. The chemical potential in the left/right lead is $\mu_{L/R}$ and $\beta = 1/k_B T$.

2.1.1 The Hamiltonian of the electron island

The general form of the Hamiltonian for n interacting electrons with spin $\sigma = \pm 1/2$ is given by

$$H_D = \sum_{m,\sigma} (\varepsilon_m - e\Phi + g\mu_B B\sigma) c^+_{m,\sigma} c_{m,\sigma} + \sum_{\substack{m_1,m_2,m_3,m_4 \\ \sigma_1,\sigma_2}} V_{m_1 m_2 m_3 m_4}\, c^+_{m_1,\sigma_1} c^+_{m_2,\sigma_2} c_{m_3,\sigma_2} c_{m_4,\sigma_1} \,. \tag{3}$$

Electrons in the non-interacting single-electron states m are created and destroyed by $c^+_{m,\sigma}$ and $c_{m,\sigma}$, respectively. The magnetic field B is taken into account by the Zeeman term in the first sum. The energies of the non-interacting electrons in the island are ε_m, $V_{m_1 m_2 m_3 m_4}$ the matrix-elements of the Coulomb interaction.

The interactions between the electrons outside the dot are neglected. The interaction between the electrons inside and outside of the dot is parametrized by an electrostatic potential $e\Phi$. It comprises the influence of the voltages applied to the leads and/or the gate, V_G [46]. This simplifying assumption is visualized in Fig. 3. It seems to be quite realistic for describing the recent experiments [30]. We find

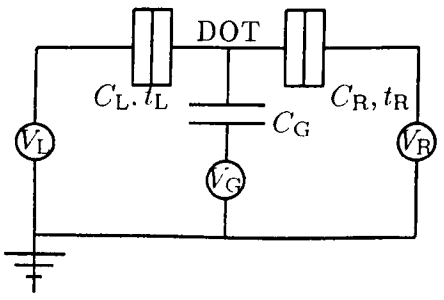

Fig. 3 Equivalent circuit for the experimental setup we have in mind. The dot region is coupled capacitively to a gate. The tunneling barriers are assumed to behave as (weakly transmissive) capacitors.

$$\Phi = \frac{C_G V_G + C_L V_L + C_R V_R}{C_G + C_L + C_R} . \tag{4}$$

The voltages applied to the leads are given by the chemical potentials via $\mu_{L/R} = -eV_{L/R}$. The bias voltage is $V = V_R - V_L$. The C's are the capacitances of the tunnel junctions and the gate capacitor, respectively. They lead to an additional influence of the chemical potentials on the eigenenergies of the dot. In all our calculations, we assumed $C_G = C_L = C_R$. Other values renormalize only the voltage scales. In the experiments, their ratios can be determined from the relative changes of voltages when tracing a given conductance peak (see Section 6.6).

Since the Hamiltonian with $\Phi = 0$ and $B = 0$ commutes with both, the potential energy $H_\Phi = \sum_{m,\sigma}(-e\Phi)c^+_{m,\sigma}c_{m,\sigma}$ and the Zeeman energy $H_B = \sum_{m,\sigma} \times g\mu_B B\sigma c^+_{m,\sigma}c_{m,\sigma}$, the latter do not change the electronic eigenstates, but they do influence the corresponding energies. Thus, we have implicitly assumed that the shape of the electronic wave functions within the dot are not influenced by the applied voltages. Only the electron number-dependent energy $-en\Phi$ has to be added. The total energy of a n-electron eigenstate $|\Psi_i^D\rangle$ is then given by

$$E_i(\Phi, B) = E_i(\Phi = 0, B = 0) - e\Phi n_i + g\mu_B B M_i , \tag{5}$$

where n_i is the number of electrons and M_i the total magnetic quantum number of the correlated state.

2.1.2 Coupling to a heat bath

The electronic system is assumed to be coupled via a Fröhlich-type coupling [47]

$$H_{ep} = \sum_{q,m_1,m_2,\sigma} \sqrt{g(q,m_1,m_2)}c^+_{m_1,\sigma}c_{m_2,\sigma}(a_q + a^+_{-q}) \tag{6}$$

to a Bosonic heat bath described by the Hamiltonian

$$H_{Ph} = \sum_q \hbar\omega_q(a^+_q a_q + \frac{1}{2}) . \tag{7}$$

Here, $\sqrt{g}$ is the coupling matrix element while a^+_q and a_q create and annihilate Bosons with wave vector q, respectively. The coupling to Bosons gives rise to transitions between the dot levels without changing the electron number. A phononic bath is a microscopic model that leads to such terms. For simplicity, we assume that the product of the matrix element $g(q, m_1, m_2)$ and the density of Bosonic states $\rho_{ph}(q)$ are independent of q, m_1 and m_2.

Furthermore, we assume that the coherence of the eigenstates of H is destroyed on the time scale of the phase coherence time τ_φ, which is much larger than the semiclassical time an electron needs to travel from one barrier to the other[1]. Thus, the motion of the electrons inside the dot is assumed to be sufficiently coherent such that Fabry-Perot-like interferences – leading to quasi-discrete levels – exist.

---

[1] It is well known that strong dissipation can suppress tunneling [48]. This choice for the phase breaking rate τ_φ^{-1} guarantees that the renormalization of the tunneling rates through the barriers is negligible.

2.1.3 Tunneling between the leads and the electron island

The barriers are represented by the tunneling Hamiltonians

$$H_{\mathrm{L/R}}^{\mathrm{T}} = \sum_{k,m,\sigma} \left(T_{k,m}^{\mathrm{L/R}} c_{\mathrm{L/R},k,\sigma}^{+} c_{m,\sigma} + h.c. \right), \tag{8}$$

where $T_{k,m}^{\mathrm{L/R}}$ are the transmission probability amplitudes. Since we want to investigate the effects that originate in the electronic properties of the island, we assume the transmission probability amplitudes in (8) to be independent of k, m and spin. Independence of k, or, equivalently, of the energy, can safely be assumed since the variations of the differential conductance can be expected on the energy scale of the quasi-discrete excitation energies of the island which is much smaller than the Fermi energy. At most, a dependence on energy could lead to slow variations in the heights of the conductance peaks. Similarly, it is reasonable to assume independence of m and σ for a tunnel barrier without any internal structure, and no spin scatterers. When attempting quantitative comparisons with experiment, these effects cannot be completely neglected. This is, however, beyond the scope of the present work.

By taking only tunneling processes in the lowest order into account, we obtain the tunneling rates to be given by Fermi's golden rule,

$$t_{\mathrm{L/R}} = \frac{2\pi}{\hbar} \sum_{k,\sigma} \left| T_{k,m}^{\mathrm{L/R}} \right|^2 \delta(\varepsilon_k^{\mathrm{L/R}} - E) \approx \frac{2\pi}{\hbar} \left| T^{\mathrm{L/R}} \right|^2 \rho^{L/R}(E) . \tag{9}$$

If they are small compared to the phase breaking rate τ_φ^{-1}, or when the temperature leads to a sufficient smearing of the initial states in the leads, the phase correlations between subsequent tunneling processes need not to be taken into account. In this limit of sequential tunneling, the non-diagonal elements of the reduced density matrix of the dot decay fast on the timescale of the tunneling events. The time evolution of the occupation probabilities of the n-electron states in the dot can then be calculated by using a rate equation taking into account only the effective transition rates between their diagonal elements P instead of the full von Neumann equation[2]. Our aim is here to deal with the sequential tunneling which yields the dominant effects observed in the present transport experiments on quantum dots. Our method is very well suited for this but does not allow to take into account resonant tunneling, for instance.

3 The method

We will explain the electronic transport properties of an electron island by considering the transitions between the n-electron eigenstates of the isolated system that correspond to different electron numbers. These transitions are induced by the coupling to leads, such that electrons can tunnel between the latter and the island. Since the coupling is assumed to be very weak, the transport properties are mainly governed by the properties of the isolated island.

[2] The necessity to treat the phase coherent version of the von Neumann equation was mentioned before [49], but was carried out only for special cases.

Our strategy consists of several steps. First, we determine the spectrum of the isolated dot. Then, we calculate the transition rates between the eigenstates of the isolated dot H_D in lowest order in the tunneling terms $H_T^{L/R}$ and in the coupling to the Bosonic heat bath H_{ep}. With these rates, a master equation yields the stationary occupation probabilities of the n-electron eigenstates. Finally, we determine the current by determining the rate of tunnel events through one of the barriers *out* of the island and subtracting the processes *into* the island through the same barrier.

Selfenergy contributions due to the coupling to the leads appear in higher orders of the tunneling term [50]. They are not taken into account. They lead to a finite width of the conductance peaks at zero temperature [51]. At temperatures larger than $t_{L/R}$ the lineshape of the peaks is essentially given by the Fermi-Dirac distribution. In experiment, it is possible to tune the barriers such that the intrinsic linewidth due to the finite tunneling rate is negligible as compared to the broadening due to finite temperature [3, 29].

This is similar to an earlier approach [52] where linear transport properties and small deviations from equilibrium were addressed without considering spin effects. In contrast to [53, 54], where the occupation probabilities of one-electron levels were considered, we consider here the populations P_i of the n-electron Fock states $|\Psi_i^D\rangle$ of H_D. This enables us to overcome the phenomenological charging model for the electron-electron interaction, and especially to include spin selection rules and general transition matrix element effects.

3.1 Energy spectrum

Starting from the isolated island, we determine first the n-electron Fock states $|\Psi_i^D\rangle$ of H_D. Each of them $|\Psi_i^D\rangle$ is associated with a certain electron number n_i, with an energy eigenvalue E_i, total spin S_i, and magnetic quantum number M_i. We will consider different models in the following sections together with the corresponding transport properties.

In order to demonstrate the approach we will discuss in Section 4 a simple two-level Anderson model. The Hubbard-like interaction term is only non-zero when both of the energy levels are occupied. In Section 5 we consider the charging model. Here, the electron-electron interaction is reduced to an electron number-dependent additive energy contribution towards the total energy. In order to include quantum effects, we use in Section 6 a Hamiltonian which describes electrons confined in a quasi-one dimensional dot including Coulomb interaction and spin. We diagonalize the Hamiltonian numerically for up to four electrons [55–57], and calculate the wave functions [58]. For small electron density (large mean distance of the electrons), the low energy excitations of the island can be obtained analytically using the 'pocket state' approximation [59]. With the latter, results were obtained for up to six electrons. The approach can also be applied to interacting electrons that are confined in a square [59]. The corresponding transport properties are described in Section 8.

3.2 Transitions between n-electron states and transport

The transitions that contribute to the current at $T = 0$ must fulfill the following conditions.

1. Energy has to be conserved (see Appendix A). An electron which tunnels into the dot has to provide the energy difference $E = E_j - E_i$ between the final and initial states with n_j and n_i electrons, respectively ($n_j = n_i + 1$). These transitions can only occur if the chemical potential in the respective lead is larger than E. Similarly, electrons which leave the dot need empty states in a lead. This requires a chemical potential below E.
2. In order to generate a net current, transitions with increasing electron number must be induced by entering from one side, and those with decreasing number of electrons by leaving to the other. At $T = 0$, this yields for the chemical potentials the condition $\max(\mu_L, \mu_R) > E > \min(\mu_L, \mu_R)$.
3. The energy difference between the ground states of successive electron numbers must be within the energy window $\max(\mu_L, \mu_R) > E > \min(\mu_L, \mu_R)$. Otherwise, the system will remain trapped in one of the ground states.[3]
4. The excited states involved in the transport must be reachable by allowed transitions starting from one of the ground states of the corresponding electron numbers. Otherwise, they are 'disconnected' and cannot contribute to the current since none of them can ever be occupied.

These rules provide a qualitative understanding of the transport properties of the electronic island. It is nevertheless necessary to perform a quantitative calculation in order to determine all of the properties of the current-voltage characteristics.

3.3 Transition rates

Due to the smallness of H^T, simultaneous transitions of two or more electrons [60, 61], which are processes of higher order in H^T, are strongly suppressed. We neglect them, consistent with the above described approximations involved in the tunneling Hamiltonian which are only reasonable for almost impenetrable barriers [45].

In lowest order in the tunneling Hamiltonian H^T, only one-electron processes occur. Further 'selection rules' will be specified below. The transition rates between states $|\Psi_i^D\rangle$ and $|\Psi_j^D\rangle$ with $n_j = n_i + 1$ are denoted by $\Gamma_{i,j}^{L/R,-}$ and $\Gamma_{j,i}^{L/R,+}$, depending on whether an electron is leaving or entering the dot through the left/right barrier, respectively. Fermi's golden rule or standard time-dependent perturbation theory (see Appendix A) yields

$$\Gamma_{i,j}^{L/R,-} = \frac{1}{2}\left|\langle S_j, M_j, \frac{1}{2}, \pm\frac{1}{2} \mid S_i, M_i\rangle_{CG}\right|^2 t_{L/R}[1 - f_{L/R}(E)]\delta_{n_i,n_j-1}\,,$$

$$\Gamma_{j,i}^{L/R,+} = \frac{1}{2}\left|\langle S_i, M_i, \frac{1}{2}, \pm\frac{1}{2} \mid S_j, M_j\rangle_{CG}\right|^2 t_{L/R} f_{L/R}(E)\delta_{n_j,n_i+1}\,. \tag{10}$$

As mentioned above, the electron has to provide the energy difference $E = E_j - E_i$. The Clebsch-Gordan coefficients $\langle ... \rangle_{CG}$ arise from the spin part of the states.

---

[3] Only at very high voltages outside the SET regime, when transitions to states with more distant electron numbers are possible, also excited states can be continuously occupied without significant population of the corresponding ground state.

They introduce spin selection rules for transitions. The factor $1/2$ accounts for the reduced density of states for a given spin direction in the leads. In particular, transition rates between states whose difference in total spin or in the magnetic quantum number is *not* $\pm 1/2$ vanish because the corresponding Clebsch-Gordan coefficients are zero. The numerical values of the squares of the Clebsch-Gordan coefficients are listed in Table 2.

The spatial part of the matrix elements associated with the transitions has been assumed to be constant in (10). Only the important and very general spin part is taken into account. It has crucial consequences when considering correlated electrons, as we will see below.

The bosonic heat bath weakly coupled to the electrons causes (inelastic) transitions between $|\Psi_i^{\mathrm{D}}\rangle$ and $|\Psi_j^{\mathrm{D}}\rangle$ without changing the electron number, the total spin and the magnetic quantum number. For small H_{ep} the rate is given by (Appendix A)

$$\Gamma_{j,i}^{\mathrm{in}} = r[n_{\mathrm{B}}(|E|) + \Theta(E)] \,. \tag{11}$$

We assume for simplicity that the product $r \equiv g\rho_{\mathrm{ph}}$ is constant. This is the lowest order, quadratic in the electron-heat bath coupling strength $\sqrt{g}$. The quantity ρ_{ph} is the boson density of states, and $n_{\mathrm{B}}(E) = (\exp(\beta E) - 1)^{-1}$ is the Bose-Einstein distribution.

The complete matrix of transition rates is $\Gamma = \Gamma^{\mathrm{L},+} + \Gamma^{\mathrm{R},+} + \Gamma^{\mathrm{L},-} + \Gamma^{\mathrm{R},-} + \Gamma^{\mathrm{in}}$.

3.4 Occupation probabilities and the current

Given the transition rates, the master equation for the time evolution of the occupation probabilities P_i of the many-electron states is

$$\frac{d}{dt}P_i = \sum_{j\,(j\neq i)} (\Gamma_{i,j}P_j - \Gamma_{j,i}P_i) \quad \text{with} \qquad \sum_i P_i = 1 \,. \tag{12}$$

One obtains the stationary *non-equilibrium* populations $\bar{P}_i$ by solving the system of linear equations for the occupation probabilities which result from assuming $dP_i/dt = 0$.

Our method allows to determine the stationary non-equilibrium populations of all the states for arbitrary bias voltage. Deviations from the equilibrium distribution linear in the applied voltage were mentioned previously [52]. In addition, the exact many-electron states including their spins can be taken into account. The calculation is not restricted to the conventional charging model. A similar method was applied in the FQHE regime but without taking into account the spin [42].

The dc-current can be calculated by considering one of the barriers separately,

$$I \equiv I^{\mathrm{L/R}} = (-/+)e \sum_{i,j\,(j\neq i)} \bar{P}_j(\Gamma_{i,j}^{\mathrm{L/R},-} - \Gamma_{i,j}^{\mathrm{L/R},+}) \,. \tag{13}$$

The first term in (13) contains the processes in which an electron leaves the island through the left/right barrier, while the second term subtracts the electrons that enter the island.

4 Anderson impurity

As a first application we consider the transport of spinless electrons through an Anderson impurity [62]. It consists of two one-electron states and a Hubbard-like interaction term that provides a 'charging energy' U when both of the levels are occupied. The populations and the current can be determined analytically. The result is a generalization of a previous investigation [50] which was dealing with the linear transport through an Anderson impurity using a Landauer-type conductance formula. The Hamiltonian H_D is given by

$$H_D^{AI} = (\varepsilon_1 - e\Phi)c_1^+ c_1 + (\varepsilon_2 - e\Phi)c_2^+ c_2 + U c_1^+ c_1 c_2^+ c_2 \,. \tag{14}$$

Here, $c_{1/2}^+$ and $c_{1/2}$ create and destroy spinless electrons in the states 1 and 2 of the impurity, respectively. The eigenstates and the corresponding energies can easily be determined (Table 1).

4.1 The transition rates

The rates for the electron tunneling and the electron-phonon scattering are determined in the Appendix A. The spin can be omitted here. The matrices $\Gamma^{L/R,+}$ have nonzero elements only when a single electron enters the dot. The possible transitions are $|\Psi_1^D\rangle \to |\Psi_2^D\rangle$, $|\Psi_1^D\rangle \to |\Psi_3^D\rangle$, $|\Psi_2^D\rangle \to |\Psi_4^D\rangle$ and $|\Psi_3^D\rangle \to |\Psi_4^D\rangle$ (the labeling of the states is introduced in Table 1). For the corresponding rates one finds

$$\Gamma_{j,i}^{L/R,+} = t_{L/R} f_{L/R}(E)\delta_{n_j,n_i+1} \,. \tag{15}$$

Matrices $\Gamma^{L/R,-}$ describe processes where an electron escapes through one of the barriers. Here, only the inverse transitions between $|\Psi_j^D\rangle$ to $|\Psi_i^D\rangle$ can occur and the electron which leaves the island has to find an empty state in the lead. Therefore, these matrices must contain Pauli blocking factors,

$$\Gamma_{i,j}^{L/R,-} = t_{L/R}[1 - f_{L/R}(E)]\delta_{n_i,n_j-1} \,. \tag{16}$$

There are only two one-electron states, $|\Psi_2^D\rangle$ and $|\Psi_3^D\rangle$, between which inelastic relaxation processes are possible. The respective rates are $\Gamma_{3,2}^{in} = r n_B(E)$ and $\Gamma_{2,3}^{in} = r[n_B(E) + 1]$ for phonon absorption and emission, respectively. The energy difference is $E = E_3 - E_2 (> 0)$.

Table 1 Electron numbers n_i, eigenenergies E_i and the eigenstates $|\Psi_i^D\rangle$ of the four states for the Anderson model (14). The 'vacuum state' $|0\rangle$ denotes the empty dot.

i	n_i	E_i	$\lvert\Psi_i^D\rangle$
1	0	0	$\lvert 0\rangle$
2	1	$\varepsilon_1 - e\Phi$	$c_1^+\lvert 0\rangle$
3	1	$\varepsilon_2 - e\Phi$	$c_2^+\lvert 0\rangle$
4	2	$\varepsilon_1 + \varepsilon_2 + U - 2e\Phi$	$c_1^+ c_2^+\lvert 0\rangle$

4.2 Stationary occupation probabilities and current

With these we construct the full matrix of transition rates by summing the contributions of all of the possible processes,

$$\Gamma = \begin{pmatrix} 0 & \zeta(\varepsilon_1) & \zeta(\varepsilon_2) & 0 \\ \xi(\varepsilon_1) & 0 & r[n_B(\varepsilon_2-\varepsilon_1)+1] & \zeta(\varepsilon_2+U) \\ \xi(\varepsilon_2) & rn_B(\varepsilon_2-\varepsilon_1) & 0 & \zeta(\varepsilon_1+U) \\ 0 & \xi(\varepsilon_2+U) & \xi(\varepsilon_1+U) & 0 \end{pmatrix}. \tag{17}$$

Here, we have defined

$$\xi(E) \equiv t_L f_L(E) + t_R f_R(E) \text{ and } \zeta(E) \equiv t_L[1-f_L(E)] + t_R[1-f_R(E)]. \tag{18}$$

By inserting (17) into the master equation (12), we obtain a system of four linear equations which can be solved analytically.

The stationary populations $\bar{P}_i$ are

$$\bar{P}_1 = (x_1 y + x_2)/\Sigma, \quad \bar{P}_2 = y/\Sigma, \quad \bar{P}_3 = 1/\Sigma, \quad \bar{P}_4 = (x_4 y + x_3)/\Sigma, \tag{19}$$

where the abbreviations

$$\Sigma = x_1 y + x_2 + y + 1 + x_4 y + x_3, \quad y = \frac{\Gamma_{2,1}x_2 + \Gamma_{2,4}x_3 + \Gamma_{2,3}}{\Gamma_{3,1}x_1 + \Gamma_{3,4}x_4 + \Gamma_{3,2}} \tag{20}$$

$$x_{\{1\}\{2\}} = \frac{\Gamma_{1,\{2\}\{3\}}}{\Gamma_{2,1}+\Gamma_{3,1}}, \quad x_{\{3\}\{4\}} = \frac{\Gamma_{4,\{3\}\{2\}}}{\Gamma_{3,4}+\Gamma_{2,4}} \tag{21}$$

were introduced.

Independent of the inelastic relaxation rate r, the stationary occupation probabilities are given by the equilibrium (Gibbs) distribution

$$P_i^G = \frac{1}{\mathcal{Z}} e^{[-\beta(E_i-\mu n_i)]} \tag{22}$$

in the limit of zero voltage, $\mu = \mu_L = \mu_R$. The inverse temperature β is equal to the one in the leads, and $\mathcal{Z}$ is the grand canonical partition function. In general, however, $\bar{P}_j$ can be drastically different from P_i^G.

The current is obtained by inserting (19) into (13),

$$\begin{aligned} I = e[&(\Gamma_{3,4}^{R,-} + \Gamma_{2,4}^{R,-})\bar{P}_4 + (\Gamma_{1,3}^{R,-} - \Gamma_{4,3}^{R,+})\bar{P}_3 + (\Gamma_{1,2}^{R,-} - \Gamma_{4,2}^{R,+})\bar{P}_2 \\ &- (\Gamma_{2,1}^{R,+} + \Gamma_{3,1}^{R,+})\bar{P}_1]. \end{aligned} \tag{23}$$

4.3 Conductance peaks

Consistent with recent results [50] for the linear transport properties of the present model, we find conductance peaks for $\mu_L = \mu_R = \mu = \varepsilon_1 - e\Phi$ and $\mu =$

$\varepsilon_2 + U - e\Phi$. They are thermally broadened by the finite width of the derivative of the Fermi functions which enter the transition rates.

In reference [50], the current was calculated using a Landauer formula which involves the density of states of the quantum dot. The latter was determined from the imaginary part of the Green's function which was calculated by solving an equation of motion including the coupling to the leads. As a consequence, the peaks in the density of states were broadened due to a self-energy contribution $\hbar t = \hbar t_L + \hbar t_R$. Here, we consider the regime $\hbar t_L, \hbar t_R \ll k_B T$, where the broadening due to the finite coupling to the leads is negligible. In this regime, we can determine the current for arbitrary voltages.

For finite transport-voltage, $V = (\mu_L - \mu_R)/e$, the peaks in the differential conductance as a function of the gate-voltage V_G (which directly enters the electrostatic potential Φ (4)) show additional structure.

In the linear regime, current can flow as long as the energy E for a ground-state-to-ground-state transition between adjacent electron numbers ($E = E_2 - E_1$ or $E = E_4 - E_2$) coincides with the chemical potentials in the leads. If this is not the case, the system remains in a ground state. The transport is completely blocked (Coulomb blockade).

At finite transport voltage, the condition

$$\mu_L \geq E \geq \mu_R \tag{24}$$

is fulfilled for a non-vanishing interval of gate-voltage. If the voltage is sufficiently large, such that in addition to the ground-state-to-ground-state transition also transitions between excited states with different electron numbers can fulfill (24), additional structure appears in the current-voltage characteristic. The current changes when the number of available transitions is changed.

This is shown in Fig. 4, where the current is plotted for different voltages. Since there are only two states with the same electron numbers $n_2 = n_3 = 1$, the additional step at $eV \geq E_3 - E_2$ is related to the transition involving the only excited state of the system, $|\Psi_3^D\rangle$. The first peak corresponds to the transitions between $|\Psi_1^D\rangle$ with $n_1 = 0$ and $|\Psi_2^D\rangle$, $|\Psi_3^D\rangle$ with $n_2 = n_3 = 1$ electron. The ground-state-to-ground-state transition is shifted to the chemical potentials and contributes to the current.

The second step arises when the gate voltage is further increased and the transition to the excited state enters the interval (24). As soon as the transition between the ground states is energetically lower than the lower one of the chemical potentials, the system is blocked in the one-electron ground state $|\Psi_2^D\rangle$, though the transition involving the excited state still fulfills (24). There is no possibility to empty the state $|\Psi_2^D\rangle$ until the gate-voltage is increased to a value for which the transition to the two electron state $|\Psi_4^D\rangle$ becomes possible. Since the ground-state-to-ground-state transition between $|\Psi_2^D\rangle$ and $|\Psi_4^D\rangle$ is energetically higher than the transition involving the excited state $|\Psi_3^D\rangle \longleftrightarrow |\Psi_4^D\rangle$, both of them come into play simultaneously, and the current jumps directly to its maximum value. On the other side of the peak, however, the current decreases in two steps because the transition which involves the excited state exits the range (24) before the ground-state-to-ground-state transition can leave. For the models with more than two single electron levels the conductance peaks will show more structure due to more possibilities for transitions.

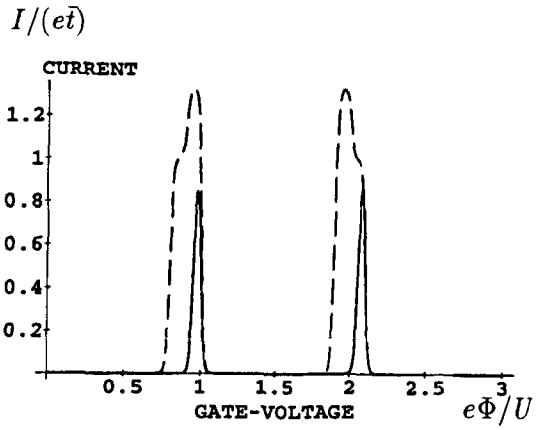

Fig. 4 Conductance peaks in the transport through an Anderson impurity as a function of the gate-voltage. The energies of the single-electron levels are $\varepsilon_1 = U$ and $\varepsilon_2 = 1.1U$ and the transmittivities of the barriers have been chosen symmetric as $t = t_L = t_R$. The temperature $k_B T = 0.01U$ is chosen considerably smaller than the level spacing. The right chemical potential is fixed at $\mu_R = 0$ and the bias voltage is $eV = 0.02U$ and $eV = 0.2U$ for the solid and the dashed line, respectively. The current is given in units of the total transmission rate $\bar{t} = t_L t_R/(t_L + t_R)$. The results are shown for $r = 0$.

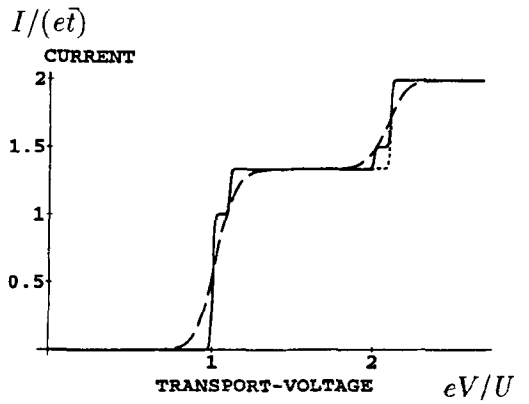

Fig. 5 Current-voltage characteristic for the transport through an Anderson impurity. The parameters are chosen as in Fig. 4. The chemical potential in the right lead and the electrostatical potential are always fixed at $\mu_R = \Phi = 0$ while the left chemical potential is varied. Temperatures are $k_B T = 0.005\,U$ and $k_B T = 0.05\,U$ for the solid and the dashed line, respectively. While the latter curves show the situation for $r = 0$, the dotted line represents $k_B T = 0.005U$ and $r = 50t$.

4.4 Current-voltage characteristic

Figure 5 shows the current-voltage characteristic obtained for the Anderson impurity. At sufficiently low temperature the two one-electron levels can be resolved. We observe finestructure in addition to the usual Coulomb steps which occur when the states with the next higher electron number become accessible.

The first step in the current occurs when the lower of the states with $n_i = 1$ can be occupied. The transition $|\Psi_1^D\rangle \longrightarrow |\Psi_2^D\rangle$ is responsible for the increase of the current. The transition energy $E_2 - E_1$ lies now between the chemical potentials in the leads. If the voltage is increased, the transition $|\Psi_1^D\rangle \longrightarrow |\Psi_3^D\rangle$ enters the region given by (24) too, and contributes to the current. There are now two possibilities to fill the empty dot. The rate for adding an electron from the lead in which the chemical potential is higher is enhanced and a second step appears in the current as a function of the voltage.

The second Coulomb step occurs when the transitions between the states with one and two electrons become accessible. First, the transition $|\Psi_3^D\rangle \longrightarrow |\Psi_4^D\rangle$ involving the excited state is 'switched on' and contributes to the current. As discussed above, the corresponding energy difference is smaller than for the ground-state-to-ground-

state transition. The additional higher step at $eV \approx 2.1U$ indicates the occupation of the ground state with $n = 2$.

4.5 Influence of the inelastic processes

It is tempting to define a voltage-dependent effective inverse temperature of the electron island by assuming that for the stationary occupation probabilities a Gibbs distribution holds with an effective chemical potential μ_{eff},

$$\beta_{ij} = \frac{\ln(P_i/P_j)}{E_j - E_i - \mu_{\text{eff}}(n_j - n_i)} . \tag{25}$$

However, this does generally not lead to a unique temperature [46] $\beta_{\text{eff}} = \beta_{12} = \beta_{23} = \beta_{34}$. It is only for zero voltage, $\mu_{\text{eff}} = \mu_{\text{L}} = \mu_{\text{R}}$, that the island is in thermal equilibrium with the leads, $\beta_{\text{eff}} = \beta$. The different effective temperatures usually increase with the transport voltage. Exceptions from this were only found for some arrangements of the chemical potentials relative to the one-particle energy levels.

Only for the effective temperature β_{23}, which is defined via the two one-electron states, the equilibrium temperature can be re-established even at high voltage. This happens, when the inelastic relaxation rate r between the two states becomes much larger than the tunneling rates through the barriers. Then, fast equilibration induced by the coupling to the bosonic heat bath leads to an equilibrium ratio of the populations. For $(r/t) \to \infty$, the β_{23} converges towards the temperature of the bath.

The only signature of the inelastic relaxation appears in the region of the second Coulomb step in the current-voltage characteristic. As discussed above, the first of the two steps is due to the transition $|\Psi_3^{\text{D}}\rangle \longrightarrow |\Psi_4^{\text{D}}\rangle$. After the second, the transition $|\Psi_2^{\text{D}}\rangle \longrightarrow |\Psi_4^{\text{D}}\rangle$ contributes to the current. It is now possible to doubly occupy the dot by starting from two different initial states.

Now, if the relaxation rate is very large as compared to the tunneling rate through the barrier connecting the dot and the lead with the lower chemical potential, the system relaxes to the lower one-electron state $|\Psi_2^{\text{D}}\rangle$ after the first electron has entered. This process is very fast on the timescale of the tunneling out of the dot. Therefore, the excited state $|\Psi_3^{\text{D}}\rangle$ is on the average almost never occupied for bath temperatures small compared with $E_3 - E_2$. As a consequence, state $|\Psi_4^{\text{D}}\rangle$, which can only be reached by transitions starting from $|\Psi_3^{\text{D}}\rangle$ in the range $E_4 - E_3 < \max(\mu_{\text{L}}, \mu_{\text{R}}) < E_4 - E_2$ cannot be occupied neither. Thus, the contribution of the transition $|\Psi_3^{\text{D}}\rangle \longrightarrow |\Psi_4^{\text{D}}\rangle$ which is responsible for the first of the two steps at about $eV \approx 2.05U$ is suppressed due to inelastic relaxation processes in the electron island (Fig. 5).

5 The charging model

As a second example we discuss the spinless charging model [37] which was also used before [52–54]. It is defined by assuming the interaction matrix elements

$$V_{m_1 m_2 m_3 m_4} = (U/2)\delta_{m_1,m_4}\delta_{m_2,m_3} . \tag{26}$$

The electron-electron interaction is taken into account via an energy which depends solely on the number of electrons in the island. Only in the metallic limit, when the electron density is very high, and the charge distribution is structureless, this can be justified by mean field arguments. Indeed, the behavior of metallic samples can be perfectly described using the charging model with a continuum of single-electron levels. Also, some of the characteristic properties of even only a few electrons in semiconducting quantum dots can be understood by using this model. The Hamiltonian is

$$H_{\mathrm{D}} = \sum_{m=1}^{N} (\varepsilon_m - e\Phi) c_m^+ c_m + \frac{U}{2} \sum_{m_1 \neq m_2}^{N} c_{m_1}^+ c_{m_1} c_{m_2}^+ c_{m_2}. \tag{27}$$

The transport properties were investigated using rate equations for the occupation of the one-electron levels. It was assumed in the first work [53] that the relative occupation probabilities of the one-electron levels equal the equilibrium value for states with the same electron number. In a subsequent paper [54] the populations were calculated correctly. Our present approach is equivalent to the one in the latter work. It has been used before for the same problem [52], and also in the FQHE regime [42]. It was pointed out that the populations of the many-electron states can deviate from equilibrium at finite transport voltage V. Deviations linear in V were also mentioned in [52]. We calculate the populations numerically at arbitrary voltage and show a variety of results for the current-voltage characteristic and the splitting of the conductance peaks.

Since the Hamiltonian contains only occupation number operators and the interaction term commutes with the kinetic energy, the n-electron states are *single* Slater determinants of one-electron states. A state $|\Psi_i^{\mathrm{D}}\rangle$ is characterized by a vector of the one-electron level occupations $p_m(i)$ $(m = 1, 2, ..., N)$ which are either one or zero. There are 2^N different states. The corresponding eigenenergies are

$$E_i = \sum_{m=1}^{N} p_m(i)(\varepsilon_m - e\Phi) + n_i(n_i - 1)U/2\,, \tag{28}$$

with the electron numbers are $n_i = \sum_{m=1}^{N} p_m(i)$.

5.1 The transition rates

The transition rates are calculated as in the case of the Anderson impurity (15, 16). As a 'selection rule', we have that transitions occur only between states that differ in the occupation p_m of only one one-electron level. This is due to the fact that only in this case transition matrix elements $\left|\sum_m \langle \Psi_j^{\mathrm{D}} \mid c_m^+ \mid \Psi_i^{\mathrm{D}} \rangle\right|^2$ between n-electron states are non-zero that correspond to adjacent electron numbers (see Appendix A). We obtain

$$\begin{aligned} \Gamma_{j,i}^{\mathrm{L/R},+} &= t_{\mathrm{L/R}} f_{\mathrm{L/R}}(E) \delta_{n_j, n_i+1} \delta_{1,(\vec{p}(j)-\vec{p}(i))^2}\,, \\ \Gamma_{i,j}^{\mathrm{L/R},-} &= t_{\mathrm{L/R}} [1 - f_{\mathrm{L/R}}(E)] \delta_{n_i, n_j-1} \delta_{1,(\vec{p}(i)-\vec{p}(j))^2}\,, \end{aligned} \tag{29}$$

where, as before, the energy $E = E_j - E_i$ is the difference between the eigenstates of the isolated dot (27).

5.2 *The stationary occupation probabilities*

The stationary (but non-equilibrium) solution of (12) was obtained for $N = 6$ by solving numerically the 2^N linear equations [37].

At zero bias voltage, the stationary state is the equilibrium. The occupation probabilities are given by a Gibbs distribution (22) with the chemical potential $\mu = \mu_L = \mu_R$. It can be shown that P_i^G solves the rate equation (12) for an arbitrary inelastic relaxation rate r.

For temperatures smaller and voltages larger than the level spacings, the stationary populations $\bar{P}_i$ deviate from their equilibrium values P_i^G. For $r \gg t_{L/R}$, when the dot-states decay very fast as compared to the tunneling, the ratios $\bar{P}_i/\bar{P}_j$ can be sufficiently well approximated by the Gibbs distribution P_i^G/P_j^G for fixed electron numbers $n_i = n_j$. This can be seen in Fig. 6 where the data points for $\ln \bar{P}_i$ versus E_i for a given n_i lie on straight lines with slope $-\beta$. This confirms the earlier assumption of a Gibbs distribution for states with a given electron number in [52, 53] in this parameter regime.

For different electron numbers $n_i \neq n_j$, $\bar{P}_i/\bar{P}_j$ can be far from equilibrium. It is impossible to scale all of the points onto one common curve by defining an effective chemical potential for the island. The linear correction to the Gibbs distribution calculated in [52] vanishes for the exact results for arbitrary transport voltages shown in Fig. 6.

5.3 *The current-voltage characteristic*

For temperatures lower than the level spacing, the current-voltage characteristic (Fig. 7) shows finestructure in the Coulomb staircase which is consistent with recent experiments [23, 31] and earlier theoretical predictions using a slightly different approach [53, 54]. In order to avoid artifacts arising from the finite number of one-electron levels we do not plot the contribution of the states with $n > 3$.

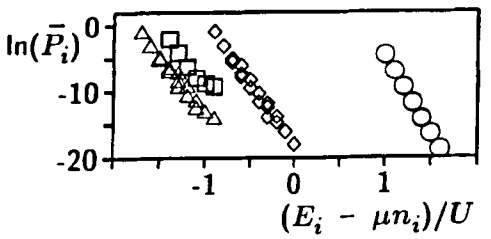

Fig. 6 Stationary occupation probabilities $\bar{P}_i$ for a dot containing $N = 6$ one-electron levels. Electron numbers are $n_i = 1$ (□), $n_i = 2$ (△), $n_i = 3$ (◇) and $n_i = 4$ (○). We used $t_L = t_R$, $\Phi = 0$, $\mu_L = 1.5U$, $\mu_R = -0.3U$ and $\mu = (\mu_L + \mu_R)/2$. Energies of the one-electron levels are $\varepsilon_1 = 0.1U$, $\varepsilon_2 = 0.2U$, $\varepsilon_3 = 0.3U$, $\varepsilon_4 = 0.4U$, $\varepsilon_5 = 0.5U$ and $\varepsilon_6 = 0.6U$. Inverse temperature is $\beta = 25/U$ and the relaxation rate $r = 100\bar{t}$. This figure is taken from [37].

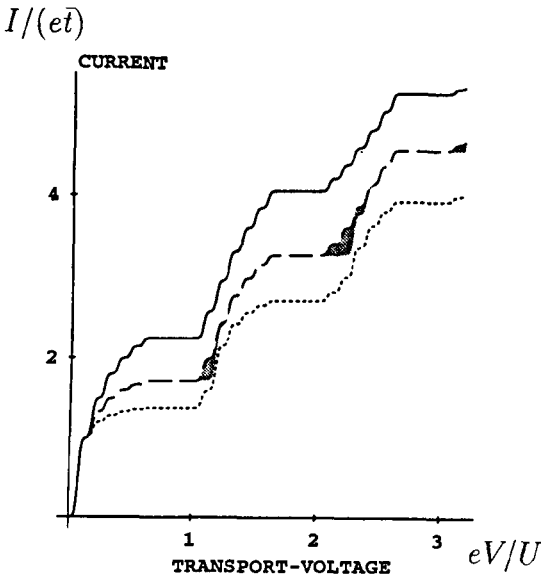

Fig. 7 Current-voltage characteristic of a dot represented by $N = 6$ one-electron levels. Model parameters are as in Fig. 6. Inverse temperature is $\beta = 100/U$ and $\mu_R = 0$, $\Phi = 0$ was chosen. Dashed lines: results for $r = 0$ and equal barriers, dotted and solid lines: $t_R/t_L = 0.5$ and 2, respectively. Shaded regions: suppressions of steps induced by relaxation $r/\bar{t} = 100$ at $t_L = t_R$. The figure is taken from [37].

Intra-dot relaxation ($\sim r$) suppresses the lowest of the finestructure steps because the electron that contributes to the current at the n-th Coulomb step has to enter the n-th or a higher one-electron level when all of the lower states become occupied via strong relaxation. For $r \gg t_{L/R}$ the $n-1$ other electrons occupy with high probability all of the lower one-electron levels.

Asymmetric coupling to the leads changes the height of the steps in the I-V curve. This can be explained for the nth Coulomb step as follows. If $t_L > t_R$ ($\mu_L > \mu_R$) the stationary occupation probabilities favor the n-electron levels, while for $t_L < t_R$ the $(n-1)$-electron states are preferred. Since there are more n-electron levels than $(n-1)$-electron levels, the probability for an electron to escape is reduced in the former case as compared to the probability for an electron to enter in the latter case. These processes limit the current. They lead to a reduction and an enhancement of the current for $t_L > t_R$ and $t_L < t_R$, respectively.

The occurrence of regions of negative differential conductance in the experiments [23, 31], however, cannot be explained within the charging model.

5.4 The conductance peaks

For fixed V, the conductance shows peaks when V_G, and thus the electrostatic potential Φ, is varied. The linear response limit simply reproduces the periodic conductance peaks in agreement with [50]. For finite bias voltage, $eV = \mu_L - \mu_R$, larger than the level spacing, transitions involving excited states can occur. The number of levels that contribute to the current varies when V_G is changed. This leads to the splitting of the conductance peaks observed experimentally, and explained qualitatively in [31, 32, 35, 36]. The experimental data [35, 36] can be explained within the 'orthodox theory' and the charging model [53, 54].

In the specific example shown in Fig. 8 correponds to $0-6-4-12-4-6-0$ allowed transitions (with increasing V_G, Section 3.2). By taking into account the sta-

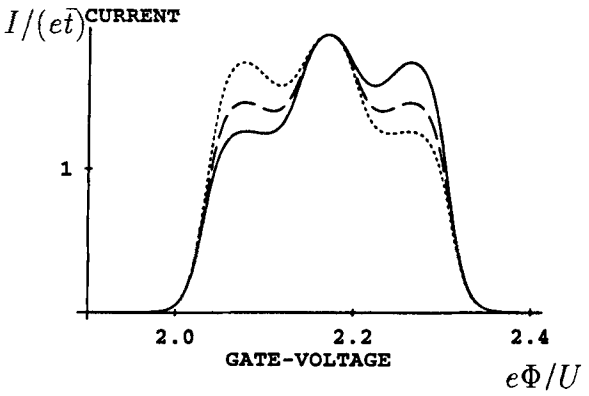

Fig. 8 Current versus V_G for $\mu_L = 0.26U$ and $\mu_R = 0$ through a dot represented by $N = 6$ one-electron levels. Model parameters are as in Fig. 6. Inverse temperature is $\beta = 100/U$. $V = 0.26U/e$ is between the double and the triple of the bare level spacing such that the conductance peaks are modulated as explained in the text. Dashed lines: results for $r = 0$ and equal barriers, dotted and solid lines: $t_R/t_L = 0.5$ and 2, respectively. The figure is taken from [37].

tionary $\bar{P}_i$'s the sequence of current values becomes $0 - 3/2 - 4/3 - 2 - 4/3 - 3/2 - 0$ [46]. If the difference $E_0(n) - E_0(n-1)$ between the energies of the n-electron ground states lies outside the interval $[\mu_R, \mu_L]$ the transport via other energetically allowed transitions is Coulombically blocked. While the relaxation rates have almost no influence on the conductance, asymmetric coupling to the leads changes the shape of the peaks considerably.

We propose to explain the slight asymmetry observed experimentally [31, 32] by the asymmetry of the barriers and we predict that the asymmetry in the finestructure of the observed conductance peaks will be reversed if the sign of the bias voltage is changed. This has indeed been observed in experiments [32]. Such asymmetric conductance properties can in principle be used to construct a mesoscopic rectifier. Similar effects were inferred earlier from the high frequency properties of mesoscopic systems containing asymmetric disorder [63].

6 Correlated electrons in quasi-one dimension

In systems with reduced dimensionality, and at low electron density, the charging model is a severe simplification for describing interacting electrons. In order to overcome its restrictions, we will consider now the the Coulomb interaction microscopically and include spin.

6.1 The energy spectrum of the electron island

We use a quasi-one dimensional (1D) square well of the length L as a model for the quantum dot. 'Exact' numerical results for up to four electrons are available [55–57]. In the limit of low density, an analytical solution exists [59] which describes the lowest excitation energies. With comparably small numerical effort much larger electron numbers can be treated by using this approach. The Hamiltonian is given by Eq. (3)

$$H_D = \sum_{m,\sigma} (\varepsilon_m - e\Phi + g\mu_B B\sigma) c^+_{m,\sigma} c_{m,\sigma} + \sum_{\substack{m_1,m_2,m_3,m_4 \\ \sigma_1,\sigma_2,}} V_{m_1 m_2 m_3 m_4}\, c^+_{m_1,\sigma_1} c^+_{m_2,\sigma_2} c_{m_3,\sigma_2} c_{m_4,\sigma_1} \,. \tag{30}$$

The interaction potential is

$$V(x,x') \propto ((x-x')^2+\lambda^2)^{-1/2}. \tag{31}$$

It is Coulomb-like for large electron distances, and cut off at small distances $|x-x'|<\lambda$ in order to avoid divergencies in the matrix elements. The cutoff parameter λ ($\ll L$) corresponds to a lateral spread of the electronic wave functions.

Since the interaction between the electrons is spin independent, the total spin S of the electrons, and its z-component, M, the total magnetic quantum number, are conserved during electron-electron scattering. They are good quantum numbers for the classification of the states. This is realistic with respect to experiments if spin-orbit scattering and other effects which are able to change the spin, are slow on the timescale of the inverse tunneling rates. In the experiments [23, 31], the order of magnitude of the current through the dot is 1 nA. This means that about 10^{10} electrons pass the dot per second. Thus, the lifetime of the spin must be larger than 100 ps in order to allow for using a spin conserving model. There is no evidence for shorter spin relaxation times in semiconductor quantum dots. Only in the presence of inhomogeneous magnetic fields induced by magnetic impurities, the spin might not be conserved. Only in these cases some of the striking results presented below might be severely affected.

The properties of the correlated states and the energy spectrum are discussed in detail in the references [55–57]. For not too large densities, when the mean separation of two electrons becomes larger than the Bohr radius a_B, $L/(n-1) > a_B$, the charge density exhibits n distinct peaks. This indicates a tendency towards Wigner crystallization [55, 58].

For very dilute electrons, $L/(n-1) \gg a_B$, the ground state is well described by a model of almost equidistant classical point charges within an interval of the length L [55]. The few correlated electrons form a 'Wigner molecule' in the island (Fig. 9, taken from [58]). For somewhat increases density, the excitation spectrum (Fig. 10) consists of well separated multiplets, each containing 2^n partially degenerate states.

The energetic differences between adjacent multiplets decrease algebraically with electron density. They correspond to vibrational excitations of the Wigner molecule. The considerably smaller intra-multiplet energy differences decrease exponentially. They are due to tunneling between different configurations of the n electrons in the well. The wave functions of individual levels within a given multiplet differ in symmetry and S.

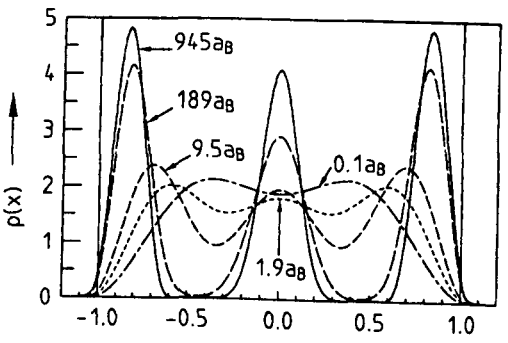

Fig. 9 The charge density $\rho(x)$ in a quasi-one dimensional dot for the ground state of $n = 3$ electrons in the dot. The corresponding system lengths L are indicated in units of the Bohr radius a_B. Clearly, for larger systems ($\rightarrow$ lower densities), there are strong deviations from the purely kinetic behavior and the interaction effects lead to distinct peaks with regions of zero charge density in between. This figure is taken from [58].

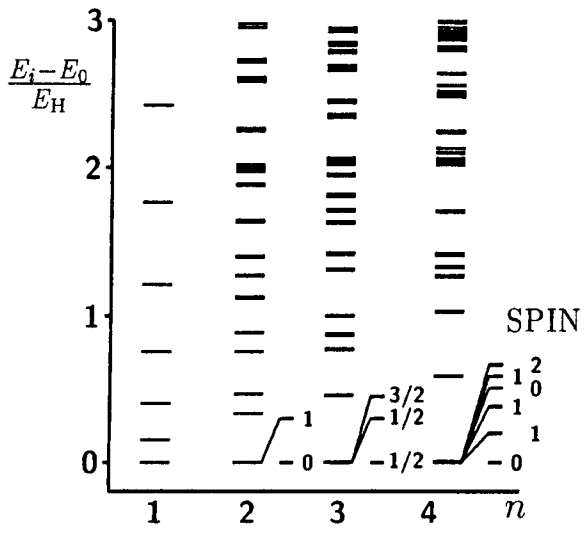

Fig. 10 The excitation spectrum of a quasi-one dimensional dot for up to four electrons in a dot of length $L = 9.45\,a_B$. For $n \geq 2$ the low lying eigenvalues form multiplets containing a total number of states being equal to the dimension of the spin Hilbert space 2^n. The lowest multiplets are magnified in order to resolve the individual states which are labeled according to their total spin. The figure is taken from [55].

For low density, the excitation energies in the lowest multiplet can be calculated [59] using a pocket state basis that takes into account the peaked structure of the wave functions. The excitation energies depend only on one tunneling integral t_n (Table 3), namely the one between adjacent configurations of the n electrons in configuration space. This tunneling integral can in principle be estimated, for instance by using the WKB approximation. It depends strongly on the cutoff parameter λ [59]. We have chosen reasonable values leading to excitation energies that are relevant for experiments.

Table 2 The squares of the vector coupling Clebsch-Gordan coefficients $\langle S_i, M_i, \frac{1}{2}, \pm\frac{1}{2} \mid S_f, M_f \rangle_{CG}$ for the combination of the total spin S_i and magnetic quantum number M_i of the dot state, with the spin 1/2 of an electron needed to form a final dot state with spin S_f and magnetic quantum number M_f. For $S_f - S_i \neq \pm 1/2$ or $M_f - M_i \neq \pm 1/2$, the Clebsch-Gordan coefficients vanish.

	$S_f = S_i + 1/2$	$S_f = S_i - 1/2$
$M_f = M_i + 1/2$	$(S_i + M_i + 1)/(2S_i + 1)$	$(S_i - M_i)/(2S_i + 1)$
$M_f = M_i - 1/2$	$(S_i - M_i + 1)/(2S_i + 1)$	$(S_i + M_i)/(2S_i + 1)$

Table 3 Spin and energies of low lying excitations of the correlated electron model at sufficiently large mean electron distances $r_s \equiv L/(n-1) \gg a_B$. The tunneling integrals t_n decrease exponentially with r_s.

n_i	S_i	$E_i - E_0(n)$
2	0	0
2	1	$2t_2$
3	1/2	0
3	1/2	$2t_3$
3	3/2	$3t_3$
4	0	0
4	1	$(1 - \sqrt{2} + \sqrt{3})t_4$
4	1	$(1 + \sqrt{3})t_4$
4	0	$(2\sqrt{3})t_4$
4	1	$(1 + \sqrt{2} + \sqrt{3})t_4$
4	2	$(3 + \sqrt{3})t_4$

Table 4 The values used in the actual calculations.

α	n_α	S_α	E_α/E_H
1	0	0	0
2	1	1/2	0.0225
3	2	0	0.2972
4	2	1	0.3572
5	3	1/2	0.9654
6	3	1/2	1.1054
7	3	3/2	1.1754
8	4	0	2.1480
9	4	1	2.2666
10	4	1	2.3939
11	4	0	2.4598
12	4	1	2.5212
13	4	2	2.5739

For the numerical calculations of the current we estimated the tunneling integrals to be $t_2 = 0.03E_H$, $t_3 = 0.07E_H$ and $t_4 = 0.09E_H$ ($E_H \equiv e^2/a_B$ is the Hartree energy). The ground state energies were determined for $L = 15\,a_B$ and $n \in \{1,2,3,4\}$ (Table 4).

In summary, two different energy scales characterize the n-electron excitations. We will demonstrate that they can in principle be detected by nonlinear transport measurements.

6.2 The transition rates

In this section we discuss the expressions for the transition rates (10).

$$\Gamma_{i,j}^{L/R,-} = \frac{1}{2}\left|\langle S_j, M_j, \frac{1}{2}, \pm\frac{1}{2} \mid S_i, M_i\rangle_{CG}\right|^2 t_{L/R}[1 - f_{L/R}(E)]\delta_{n_i,n_j-1}\,,$$

$$\Gamma_{j,i}^{L/R,+} = \frac{1}{2}\left|\langle S_i, M_i, \frac{1}{2}, \pm\frac{1}{2} \mid S_j, M_j\rangle_{CG}\right|^2 t_{L/R} f_{L/R}(E)\delta_{n_j,n_i+1}\,. \tag{32}$$

They are calculated in Appendix A and contain Clebsch-Gordan coefficients (Table 2) which account for the combination of the spin of the incoming or outgoing electron with the spin of the initial state to generate the spin of the final state. They introduce 'spin selection rules'. The quantum numbers S and M, denoting the total spin and the total magnetic quantum number of the correlated electrons in the island, respectively, can only be changed by $\pm 1/2$ when one electron enters or leaves. The spin selection rules are a consequence of using the exact correlated n-electron states in the rate equation (12). They represent drastic restrictions for the transitions, and are completely different from the 'selection rules' in the charging model, where only processes are allowed, in which one electron enters or leaves one-electron states. Here, the correlated n-electron states are linear combinations of many Slater determinants which contain contributions of all of the one-electron states.

If the exact eigenstates are known, one can determine the overlap matrix element of a state which is generated by applying an one-electron creation operator to an n-

electron state with an $n+1$-electron state [64], $\langle \Psi_j^{\mathrm{D}} \mid c_{m,\sigma}^{+} \mid \Psi_i^{\mathrm{D}} \rangle$ ($n_j = n_i + 1$). They enter the transition rates (see Appendix A) weighted with the tunneling matrix elements. They depend strongly on the details of the microscopic realization of the quantum dot such as impurities and the geometrical form. The spin effects yield very general selection rules. In first approximation, we use solely the selection rules induced by the spin part and ignore the influence of the spatial part of the wave functions. We discuss the latter in Section 6.7.

In any case, the correlations play an important role for the transport properties. The order of the levels with different spins on the energy axis is strongly influenced by the electron-electron interaction. Together with the spin selection rules it influences qualitatively the transport properties. In addition to the Coulomb blockade, further blocking effects occur, as will be discussed in the following.

6.3 The effective master equation

At zero magnetic field the states with different magnetic quantum numbers M_i are degenerate. Their stationary populations do not depend on M_i but only on S. We define the total occupation probability

$$P_{\alpha}^{\mathrm{T}} = \sum_{M=-S_\alpha}^{+S_\alpha} P_{\alpha,M} = (2S_\alpha + 1) P_{\alpha,M} \,, \tag{33}$$

where the index α contains all of the quantum numbers necessary for characterizing the state, except M. Then, the master equation (12) becomes

$$\frac{d}{dt} P_{\alpha}^{\mathrm{T}} = \sum_{\beta\,(\beta \neq \alpha)} (\Gamma_{\alpha,\beta}^{\mathrm{T}} P_{\beta}^{\mathrm{T}} - \Gamma_{\beta,\alpha}^{\mathrm{T}} P_{\alpha}^{\mathrm{T}}) \tag{34}$$

where the total transition rates

$$\Gamma_{\alpha,\beta}^{\mathrm{T}} = \sum_{M_1=-S_\alpha}^{+S_\alpha} \sum_{M_2=-S_\beta}^{+S_\beta} \frac{\Gamma_{\alpha M_1;\beta M_2}}{2S_\beta + 1} \tag{35}$$

are averages over the rates between the individual levels. Since the states with different M are degenerate, the only M-dependence is contained in the Clebsch-Gordan coefficients such that the total transition rates are

$$\Gamma_{\beta,\alpha}^{\mathrm{L/R},-} = \gamma_{\beta,\alpha}\, t_{\mathrm{L/R}} [1 - f_{\mathrm{L/R}}(E)] \delta_{n_\beta, n_\alpha - 1} \,,$$

$$\Gamma_{\alpha,\beta}^{\mathrm{L/R},+} = \gamma_{\alpha,\beta}\, t_{\mathrm{L/R}} f_{\mathrm{L/R}}(E) \delta_{n_\alpha, n_\beta + 1} \,, \tag{36}$$

with the spin dependent prefactors

$$\gamma_{\beta,\alpha} = \sum_{M_1=-S_\alpha}^{+S_\alpha} \sum_{M_2=-S_\beta}^{+S_\beta} \frac{1}{2} \left| \langle S_\alpha, M_\alpha, \frac{1}{2}, \pm\frac{1}{2} \mid S_\beta, M_\beta \rangle_{\mathrm{CG}} \right|^2 . \tag{37}$$

By evaluating the sums using the values from Table 2 one finds

$$\gamma_{\beta,\alpha} = \frac{S_\alpha + 1}{2S_\alpha + 1} \delta_{S_\beta, S_\alpha + 1/2} + \frac{S_\alpha}{2S_\alpha + 1} \delta_{S_\beta, S_\alpha - 1/2} , \tag{38}$$

which was used in reference [24]. These spin dependent prefactors favor an increase of the total spin of the electrons in the quantum dot.

Transitions due to electron phonon scattering events conserve both, total spin and magnetic quantum number as well as the number of electrons in the island. Therefore, there are not many transitions available for this kind of processes and the influence of inelastic processes is even weaker than in the charging model. In all of the calculations, we shall use $r = \bar{t} \equiv (t_L + t_R)/2$.

6.4 The current-voltage characteristics

The stationary occupation probabilities are obtained similarly as for the charging model. They are modified by spin effects.

The current-voltage characteristic calculated by using the excitation energies of Table 4 is shown in Fig. 11. First, we observe that the lengths of the steps in the Coulomb staircase, and accordingly the distances of the conductance peaks are no longer equal since the ground state energy is not proportional to $n(n-1)$ as in the charging model for small ε_m's. The deviation from the classical behavior is related to the inhomogeneity of the quantum mechanical charge distribution in the ground state [55, 57, 58]. Second, the heights of the finestructure steps appear to be more random as com-

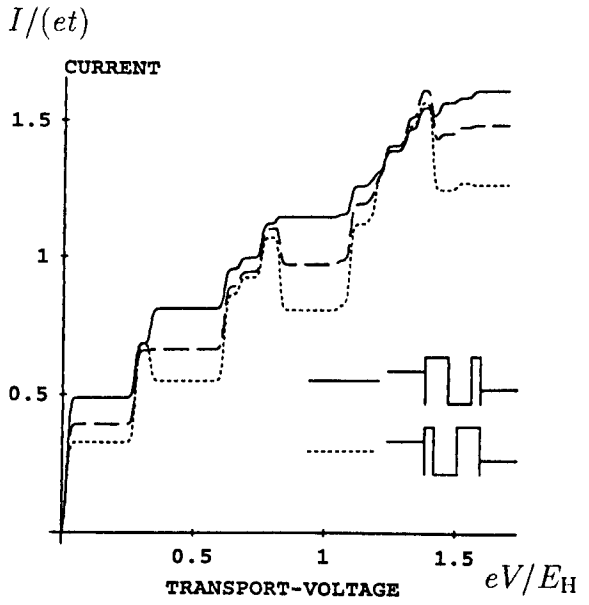

Fig. 11 Current-voltage characteristic ($\mu_R = 0$, $\Phi = 0$) of a dot described by the quasi-one dimensional correlated electron model with energy values from Table 4 for inverse temperature $\beta = 200/E_H$ and $r = \bar{t}$. Dashed, dotted and solid lines correspond to different ratios of coupling to the leads with $t_R/t_L = 1$, 0.5 and 2, respectively.

pared to those in Fig. 7 due to the non-regular sequence of total spins (cf. Table 3), and the spin dependent prefactors in the transition rates. Certain finestructure steps in the I-V characteristic may even be completely suppressed.

6.5 The spin blockade type I

Strikingly, regions of negative differential conductance occur in Fig. 11. They are induced by the reduced probability for the states of maximal spin $S = n/2$ to decay into states of lower electron number via transitions

$$n;\, S \longrightarrow n-1;\, S'. \tag{39}$$

If $S = n/2$, $S' = S - 1/2$ is the only possible final spin at the lower electron number $n - 1$. This 'spin blockade' effect will now be explained in some detail. A second kind of spin blockade is due to states with high (not necessarily maximum) total spin being the ground state or energetically close to it. This occurs for higher dimensions and will be discussed in Section 8.

For the quasi-1D model, the states with maximum spin occur only once in each multiplet for given electron number. Therefore, only one finestructure step with negative differential conductance – the current decreases with increasing voltage – can occur within each Coulomb step.

The drop in the I-V curve becomes less pronounced if $t_L < t_R$ ($\mu_L > \mu_R$). Then, the dot is mostly empty and the $(n-1) \rightarrow n$ transitions determine the current. On the other hand, if $t_L > t_R$, the spin selection rule reduces the probability for some of the $n \rightarrow (n-1)$ transitions, the negative differential conductance becomes more pronounced (Fig. 11).

To illustrate this, we concentrate on the region of negative differential conductance in the third conductance peak around the voltage $eV/E_H \approx 0.8$. This is high enough to allow for all of the transitions between the states with lower electron numbers $0 \leq n \leq 2$. The steps in the current when the voltage is increased (Fig. 11) occur when additional transitions between two states with $n = 2$ and $n = 3$ become energetically allowed. Figure 12 shows that each step in the current is accompanied by a change in the stationary occupation probabilities of the corresponding states.

In order to understand the features in more detail, we show the energy levels for $n = 2$ and $n = 3$ together with the corresponding spin-allowed transitions in Fig. 13. The chemical potential in the right lead is fixed at $\mu_R = 0$ such that at $T = 0$ electrons can leave the dot to the right side with any positive energy. This means that all of the decays to lower electron numbers are possible by tunneling through the right barrier. The chemical potential in the left lead is now increased, thus making electrons available at energies up to μ_L. A transition between an n-electron state with energy E_α and an $n+1$-electron state with energy $E_\beta > E_\alpha$ can contribute to the current when $V \equiv \mu_L/e = (E_\beta - E_\alpha)/e$.

For smaller μ_L, only the states with $n \leq 2$ can be occupied. As soon as the voltage is sufficiently high ($eV/E_H \approx 0.6$) to allow for the $n = 2 \rightarrow 3$ transition that needs the lowest amount of energy, $\mu_L = E_c - E_b$, the lowest state with $n = 3$ (**c**) acquires a finite population. This happens at the expense of the highest state for $n = 2$ (**b**) which is depopulated by this process. At the same time, the 2-electron ground state (**a**) slightly gains occupation because the ground state with $n = 3$ (**c**) can decay into

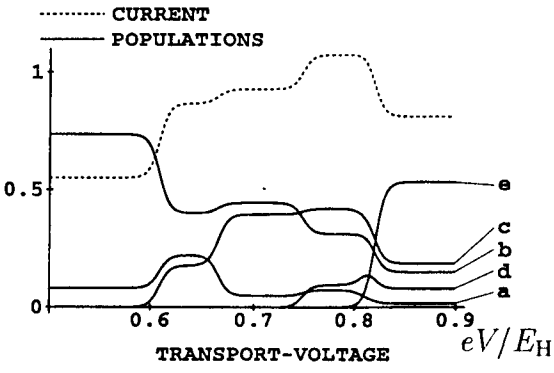

Fig. 12 The most prominent feature in Fig. 11 for $t_L > t_R$ is enlarged. The current in units of $e\bar{\Gamma}$ (dotted) and the populations of the most relevant dot states **a**: $n = 2$, $S = 0$, **b**: $n = 2$, $S = 1$, **c**: $n = 3$, $S = 1/2$ (ground state), **d**: $n = 3$, $S = 1/2$ (first excited state), **e**: $n = 3$, $S = 3/2$ versus bias voltage are shown. The populations shown here do not sum up to unity because of the occupation of other states.

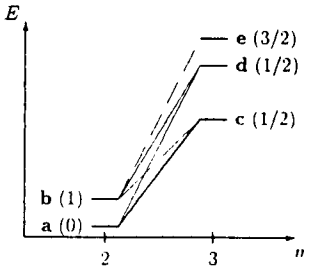

Fig. 13 Dot states for $n = 2$ and $n = 3$. The total spins S of the states are indicated in brackets next to the lines representing the level. Transitions being allowed by the selection rules are sketched. In linear transport, only the ground state to ground state transition (solid line) contributes to the conductance. At finite transport voltage, additional transitions between excited states contribute. Since the transition to the highest state (dotted-dashed) is a 'dead end', the current is reduced when the voltage is raised to a value that allows the system to enter state **e**.

this state of lower electron number. At the next step, the ground-state-to-ground-state transition becomes accessible in both directions. Then, at the step near $eV/E_H \approx 0.75$, the transition from state **b** to **d** comes into play, accompanied by further decreasing the population of the excited 2-electron state **b**, and populating the first excited 3-electron state (**d**). All of these are accompanied by an increase of the current.

For voltages slightly higher than $eV/E_H \approx 0.8$, the transition to the energetically highest state with $n = 3$ (**e**) becomes available. This state attracts considerable stationary occupation probability at the expense of all the other populations. It can only decay into a 2-electron state with $S = 1$, in contrast to the other 3-electron states (**d**, **e**). They can decay at least into two different 2-electron states. Thus, due to the 'spin selection rule', the electron has a reduced probability to leave the spin-polarized state **e**. The lifetime of this state is exceptionally large which leads to a high population. The current decreases because the total number of transitions per unit of time is decreased (by at least a factor of two in this case).

For asymmetric barriers, when the tunneling rate through the right barrier, t_R, is lower than t_L, transitions accompanied by decreasing electron number are relatively slow. The transition into the 'dead end' **e** becomes almost a 'one way road' and the 'spin blockade' is drastically enhanced (Fig. 11). If, on the other hand, processes with decreasing electron number are fast, $t_R > t_L$, the state (**e**) loses its trap-like character. The spin blockade is suppressed.

Negative differential conductances can be observed in the experimental data [23, 31] but certainly need further, much more elaborate investigations. They can in principle be used to construct a mesoscopic oscillator. The experimental observation of the influence of asymmetric coupling to the leads [32] is consistent with our above results.

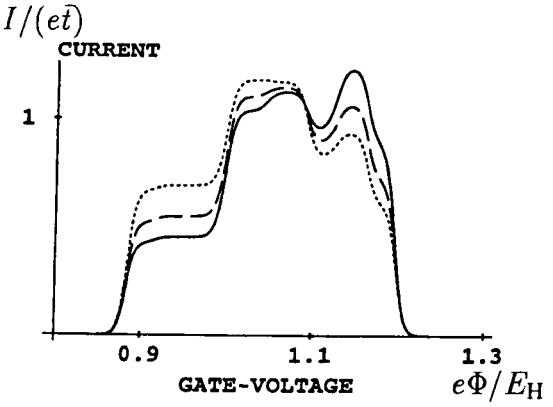

Fig. 14 The splitting of the fourth conductance peak at $\mu_L = 0.3E_H$ and $\mu_R = 0$ of a dot described by the correlated electron model (parameters as in Fig. 11). Dashed, dotted and solid lines correspond to $t_R/t_L = 1$, 0.5 and 2, respectively.

The splitting of the conductance peaks (Fig. 14) shows similar features as for the charging model. However, the periodicity and regularity of the peaks is lost due to the more irregular sequence of total spins anthe changes in the transition rates. We expect that for higher electron numbers, say $n \approx 20$, the more regular shape should be re-established. The dependence on the asymmetry of the barriers discussed in Section 4.3, however, remains the same.

6.6 Transport spectroscopy

The spectra of arrays of quantum dots were investigated by using infrared absorption spectroscopy [17–19]. This probes only the center of mass motion which, according to Kohn's theorem [21], decouples completely from the other degrees of freedom in parabolically confining potentials. It is very difficult to observe correlation effects by using this technique.

On the other hand, nonlinear transport experiments are a powerful tool to investigate the energy spectra of interacting electrons in quantum dots. The non-linear current reflects the transitions between all of the states of the dot. The influence of the electron-electron correlations on the spectra is crucial for the results. In principle, the addition spectrum can be deduced from the experimental data [23, 29]. It is therefore possible to study systematically interacting few-electron systems by this method since not only center of mass excitations are important.

To gain more insight on the structure of the conductance peaks, we plot the differential conductance $\partial I/\partial V$ as a function of the transport voltage V and the gate voltage V_G. Such a representation of data [23] together with the investigation of the influence of a magnetic field provides reliable information about the spectral properties.

6.6.1 Expected peaks

A transition $|\Psi_i^D\rangle \leftrightarrow |\Psi_j^D\rangle$ with different electron number $n_j = n_i + 1$ can contribute to the current if their energetic distance $E = E_j - E_i$ satisfies $\min(\mu_L, \mu_R) < E < \max(\mu_L, \mu_R)$. At $T = 0$, the current can change only at the lines $\mu_L = E$ or $\mu_R = E$ in the V-V_G plane. For $\mu_L = 0$ and $eV = \mu_L - \mu_R = -\mu_R$ they are given by

$$\frac{e}{C_\Sigma}(C_G V_G + C_R V) = E_0 \quad \text{and} \quad \frac{e}{C_\Sigma}(C_G V_G - (C_L + C_G)V) = E_0 . \tag{40}$$

Here, E_0 is the energy difference at $\Phi = 0$ and $C_\Sigma = C_L + C_R + C_G$ the total capacitance. The slopes of the lines depend only on the properties of the circuit (the ratios of the capacitances) while the separations reflect the excitation energies of the dot, and C_G. For simplicity, we assume $C_L = C_R = C_G$.

6.6.2 Differential conductance

The overall behavior of the differential conductance as a function of the gate- and the transport-voltage, V_G and V, is shown in Fig. 15 in a greyscale representation. Along the axis $V = 0$ the linear conductance peaks [26] can be observed at distances given by the Coulomb blockade energy. Lines that intersect at the positions of the peaks of the linear conductance correspond to ground-state-to-ground-state transitions. The regions of the Coulomb blockade are the grey, diamond shaped areas enclosed by these lines. The lines parallel to the edges of the Coulomb blockade areas reflect the spectrum of the quantum dot [29, 38, 40]. Qualitatively similar features have been observed experimentally [23, 29]. In Fig. 15 the energy spectrum given in Table 4 was used.

When either V_G or V are varied, the dot states that are involved in the transport change. At $T = 0$, this leads to steps in the current. Finite transport voltage V broadens the corresponding conductance peaks. The resulting finestructure is characteristic for the spectrum of the electron island. It is in general asymmetric [31, 35, 36].

The asymmetry is reversed when reversing the voltage [37] if the barriers are not equally transparent, in agreement with experimental findings [32]. Bright regions that correspond to negative differential conductances occur preferably when the lower chemical potential is attached to the less transmitting barrier and the transitions of the type (39) limit the current. This is shown in Fig. 16, consistent with experimentally observed asymmetries [23, 29, 31].

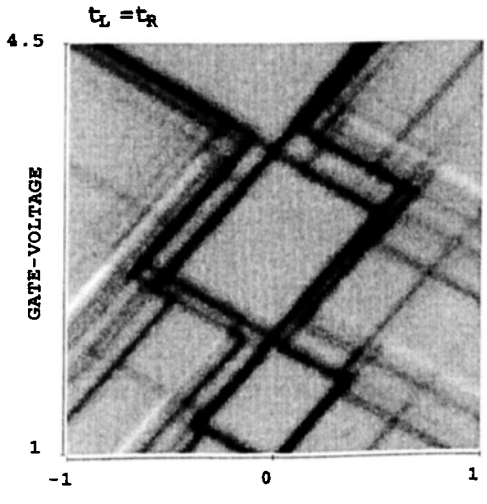

Fig. 15 Differential conductance versus gate-V_G and transport-voltage V in units of E_H/e for symmetrical coupling to the leads. The zero value inside the diamond-shaped Coulomb blockade regions corresponds to grey. Dark and bright parts indicate positive and negative differential conductances, respectively.

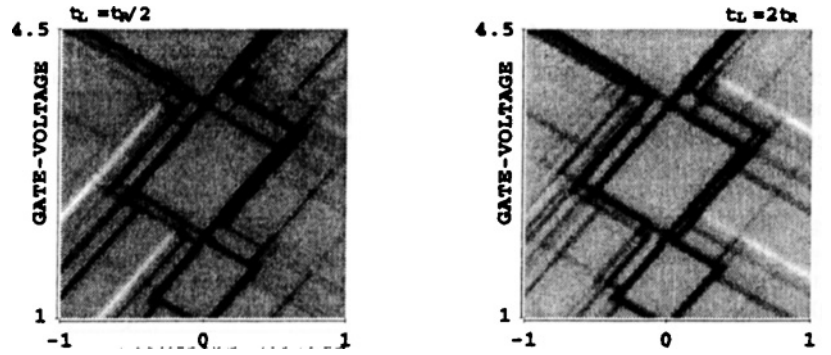

Fig. 16 Differential conductance versus gate-voltage V_G and transport-voltage V in units of E_H/e. The zero value inside the diamond shaped Coulomb blockade regions corresponds to grey. Dark and bright parts indicate positive and negative differential conductances, respectively. The couplings between the dot and the leads have been assumed to be $t_L = t_R/2$ (left) and $t_L = 2t_R$ (right). Thus, the transitions through the left/right barrier limit the current and bright regions occur mainly when the less transmitting barrier is attached to the lower of the chemical potentials.

6.7 The influence of the spatial part of the transition matrix elements

As shown above, the spin part of the transition matrix elements leads to non-trivial effects. It can be expected, that also the spatial part of the wave functions influences the current-voltage characteristic. For interacting electrons in a quasi-1D island, the exact transition matrix elements between the states corresponding to different electron numbers (10) were numerically calculated [64]. When one assumes that $T_{k,l} \equiv T$ in the tunneling Hamiltonian, the quantity to be calculated is $\left|\sum_{l,\sigma}\langle\Psi_j^D \mid c_{l,\sigma}^+ \mid \Psi_i^D\rangle\right|^2$ (see Appendix A). These matrix elements contain also the spin selection rules.

Figure 17 shows that the spatial part of the transition matrix elements reduces some of the features in the results by additionally suppressing some of the lines.

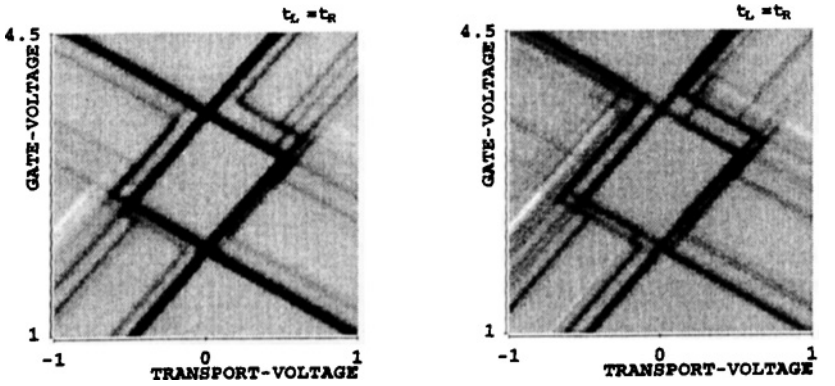

Fig. 17 Differential conductance through a quasi-one dimensional quantum dot is calculated taking into account the exact transition matrix elements between the many-electron dot states and plotted as a function of the gate- and the transport-voltage in units of E_H/e (left). For comparison, the result using only the spin Hilbert space part in determining the transition rates is shown (right). Only transitions between states with 2, 3, and 4 electrons in the dot have been taken into account.

However, the qualitative aspects remain unchanged. In particular, the spin-induced negative differential conductances are not removed.

The spatial properties depend sensitively on the specific realization of the sample. In our example, there are strong fluctuations in the values of the matrix elements for different transitions. This results in the suppression of some transitions between n-electron states *in addition* to the spin induced features but also the occurrence. On the other hand, some lines are enhanced [64] due to the changed distribution of populations. Similar effects have been proposed for an isotropic island [65] in order to explain the comparatively low number of transitions seen in experiment [23].

At present, the importance of the spatial part of the transition matrix elements is not quantitatively understood [64]. Such an investigation would require a more realistic model. We find that the main features discussed above are not affected.

7 Magnetic field effects

Investigating the influence of a magnetic field can provide more information about the electronic states. In particular, the Zeeman effect lifts the degeneracy between states with different magnetic quantum numbers. The predictions of the spin blockade theory can be compared with experiment in more detail.

In the experiments of reference [43] the field was applied parallel to the 2D electron gas, along the direction of the current. This influences only weakly the spatial part of the electron wave functions as long as the magnetic length remains large as compared to the thickness of the electron layer.

The Zeeman splitting of the energy levels is the main effect observed in the transport spectra [23, 29, 43]. Two slopes characterize the dependence of the excitation energies on the magnetic field [23, 43]. A sufficiently strong magnetic field causes a change of the spins of the ground states. This may occur either in the n or in the $n-1$ electron ground state. The result is an oscillatory dependence of the positions of the peaks in the linear conductance on the magnetic field, as reported previously [34]. In latter experiment, a gate tip was used in order to define the electron island. Although its geometry has not been completely clarified, the experimental results suggest that the Zeeman splitting is the main effect of the magnetic field, at least for low field strengths.

The Zeeman energy is given by

$$H_Z = \sum_i g\mu_B B M_i |\Psi_i^D\rangle\langle\Psi_i^D| . \tag{41}$$

It has to be added to the Hamiltonian (3). Here, g is the Landé factor, μ_B the Bohr magneton, B the magnetic field, and M_i the magnetic quantum number of the state $|\Psi_i^D\rangle$. The Zeeman term leads to a splitting of the energy levels of the states which differ only in M, and are degenerate in the absence of a magnetic field. The dependence of the energies of the 2- and 3-electron states on the magnetic field is shown schematically in Fig. 18.

Outside the quantum dot, the magnetic field changes only slightly the density of states at the Fermi energy for the different spin directions. The Fermi energy itself which is pinned by the externally applied voltages is not modified. In the experimen-

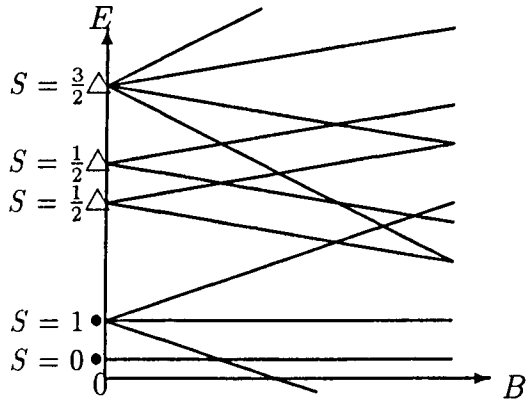

Fig. 18 The energy dependence of dot states for $n_i = 2$ (•) and $n_i = 3$ (△) on the magnetic field (schematically). The Zeeman splitting leads to level crossings and therewith changes the ground state.

tally relevant region, $E_F \gg g\mu_B B$, the effect of the magnetic field on the densities of states can be neglected.

7.1 Linear transport

Only the ground states determine the linear transport at zero temperature. The dependence of the ground-state-to-ground-state transition energy on the magnetic field is clearly reflected in the numerical results of Fig. 19 where the differential conductance as a function of the gate-voltage and the magnetic field at zero bias-voltage is shown.

The results show clearly the oscillatory behavior of the peak position as a function of the magnetic field as observed experimentally [34]. At high magnetic fields, the spin polarized states become the ground states for all electron numbers, leading to a decreasing energy difference with increasing magnetic field.

Since in the 1D model the ground state spin at $B = 0$ is zero or $1/2$ depending on the parity of the electron number, the energy difference between ground states decreases with increasing B at low field strengths if the lower electron number is even.

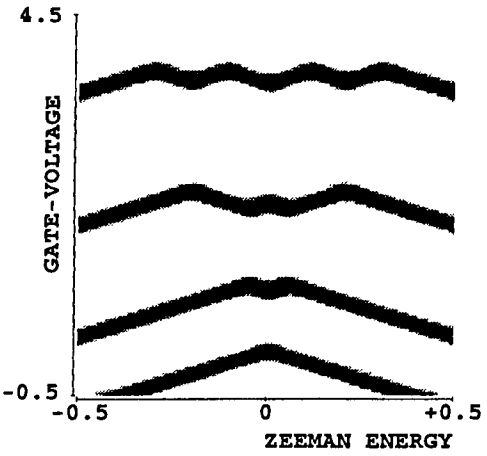

Fig. 19 Differential conductance at zero bias voltage as a function of the Zeeman energy $g\mu_B B$ and the gate-voltage in units of E_H and E_H/e, respectively.

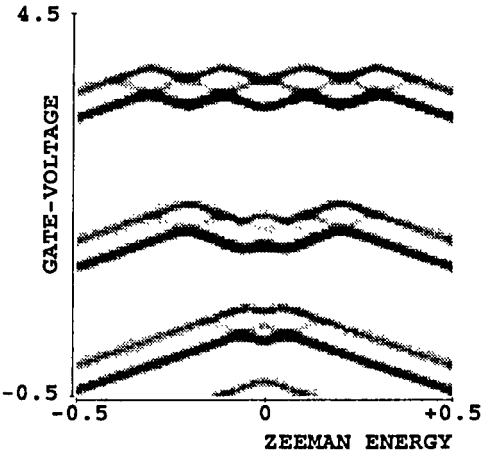

Fig. 20 Differential Conductance at bias voltage $V = 0.1\,E_H$ as a function of the Zeeman energy and the gate-voltage in units of E_H and E_H/e, respectively.

If, on the other hand, the lower of the two electron numbers is odd, the energy difference increases and the corresponding conductance peak moves to higher gate-voltage. This parity effect is shown in Fig. 19.

7.2 Finite voltage

Results for finite voltages, involving also excited states, are shown in Fig. 20. The differential conductance as a function of the gate- and the transport-voltage shows how the energies $E_j - E_i$ of the transitions between (excited) states $|\,\Psi_i^D\rangle$ and $|\,\Psi_j^D\rangle$ with different electron numbers $n_j = n_i + 1$ change with the magnetic field.

In our model, the signs of the shifts of the lines with nonzero differential conductance on the axis of the gate voltage are directly related to the signs of $\Delta M \equiv M_j - M_i = \pm 1/2$.

Since the magnetic field changes the energies of the eigenstates of the island the weights of some of the transitions are changed correspondingly. Most spectacular effects of this kind are observed for transitions which are pushed into the Coulomb blockade regions by the magnetic field. They become completely suppressed (Fig. 20).

Furthermore, the spin blockade is suppressed by a magnetic field. The condition is that the Zeeman energy exceeds the level spacing. This is consistent with recent experiments [29], where, due to the two-dimensionality of the dot, the states with highest spin are not simultaneously also the energetically highest at zero magnetic field, and the negative differential conductances appear quite close to the linear regime [23]. Then, the Zeeman splitting needed to suppress the negative differential conductance is lower (see below).

8 Two-dimensional square dots

In this section, we present results for a 2D quantum dot. As a model we use a square shaped, hard wall confinement potential. In the low density regime the low energy excitation spectrum was calculated for Coulombically interacting electrons with spin [59]. In the following, the results for up to five electrons are used. The low energy

excitation spectrum is qualitatively different from the 1D case. States with high spin can occur at low energies. The ground state is not necessarily a state with minimum spin. This leads to other types of spin blockade effects.

8.1 Spin blockade type II

The 'spin blockade type I' is related to the occupation of states with maximum spin $S = n/2$ and appears at voltages of the order of their excitation energies. These states occur both in 1D [55–57] and in 2D [59] quantum dots.

The 'spin blockade type II' is related to states with high (not necessarily maximum) spin being the ground state or energetically close to the ground state [38]. It can occur even in linear transport if the total spins of ground states that correspond to successive electron numbers differ by more than 1/2,

$$(n, \text{ground state}, S) \longrightarrow (n-1, \text{ground state}, S') \qquad |S - S'| > 1/2 . \quad (42)$$

Then, the electron island is blocked in the n- or the $n-1$-electron ground state and the corresponding peak in the linear conductance vanishes at zero temperature.

Figure 21 shows the grey scale plot of the differential conductance. One prominent feature is the missing of the linear conductance peak corresponding to the transition between 4 and 5 electrons, since the spins of the ground states are $S = 0$ ($n = 4$) and $S = 3/2$ ($n = 5$). Either finite transport voltages or finite temperatures can re-establish the conductance via transport through excited states with spins $S = 1$ ($n = 4$) and $S = 1/2$ ($n = 5$). The voltage- or temperature-induced recovery of the conductance is shown in Fig. 22. Such a feature was indeed observed experimentally [34]. Since the Lieb and Mattis theorem [68] guarantees that in 1D the spins of the ground states are always 0 or 1/2, the 'spin blockade type II' (42) is specific for 2D quantum dots. In a 'slim' dot no linear conductance peak should be missing.

In addition, states with high spins, but not necessarily completely spin-polarized, which are energetically close to the ground state, can cause blocking phenomena at $T = 0$. This is demonstrated for the transition between $n = 3$ and $n = 4$ in Fig. 23a. In contrast to the spin blockade of the first kind, (42) can lead to negative differential

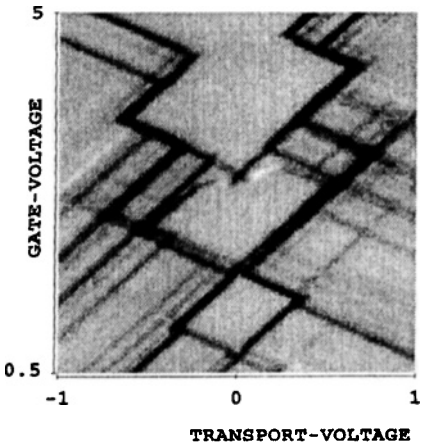

Fig. 21 Differential conductance versus gate-voltage V_G and transport-voltage V in units of E_H/e. The spectrum for a 2D square dot is used. The transition between the ground states for $n = 4$ and $n = 5$ is forbidden by the spin selection rules and the corresponding lines that should cross on the V_G-axis are missing.

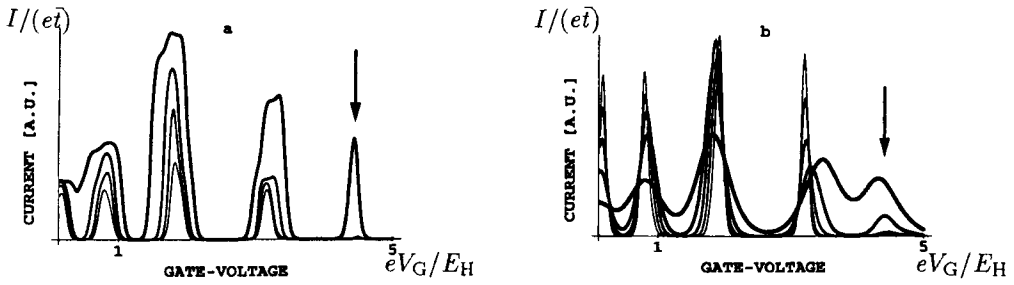

Fig. 22 Current versus gate voltage for a square quantum dot. In a) the transport voltage is increased. According to the thickness of the lines, it takes the values $V = 0.04, 0.06, 0.1, 0.2E_H/e$. In b) the temperature is increased. Thin to thick lines correspond to $\beta E_H = 100, 80, 60, 40, 20$. The missing peak in linear conductance corresponding to oscillations between $n = 4$ and $n = 5$ electrons is recovered. The peak corresponding to the transition between $n = 3$ and $n = 4$ electrons behaves unnormally because the ground-state-to-ground-state coupling is very weak and the increased temperature/voltage allows to involve excited levels.

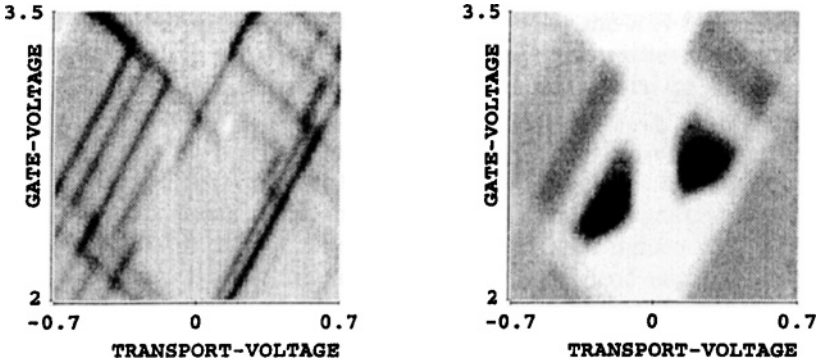

Fig. 23 Left: region around the transition between $n = 3$ and $n = 4$, magnified and with the energy of the $S = 3/2$ state being degenerate with the $n = 3$ $S = 1/2$ ground state. At low but finite transport voltage the $S = 3/2$ ground state becomes populated. Transitions to the $n = 4$ ground state are spin forbidden. Negative differential conductances appear. Right: same region but now showing the population of the $n = 3$, $S = 3/2$ state (**b** in Fig. 24 in dark. If the transport voltages are sufficient to occupy the $S = 3/2$ state it is easily populated but depopulation is difficult.

conductances even close to the peak in the linear conductance. The reason is that the $n = 3$-state with $S = 3/2$ is almost degenerate with the $S = 1/2$-ground state.

The most important energy levels are shown schematically in Fig. 24. Within the Coulomb blockade region all transition rates that increase the electron number are exponentially small. At $V = 0$ the system is in thermal equilibrium and the 3-electron ground state is populated. Already a slightly increased voltage changes the ratio between certain rates by orders of magnitude, favoring the occupation of the $S = 3/2$ state **b** (cf. Fig. 23b). This is due to a delicate interplay between multiple transitions that connect eventually the lowest $n = 3$ states via at least three intermediate states. There is a competition between processes like **a**→**d**→**c**→ **e**→**b** and the process **b**→ **e**→**a**. Direct transitions from the $S = 3/2$ state to the $n = 4$ ground state are spin forbidden. This causes the pronounced negative differential conductance at low voltages.

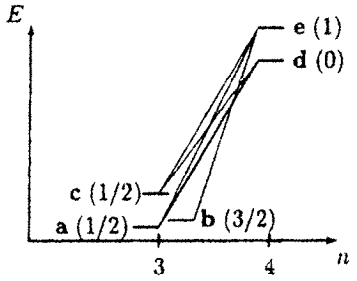

Fig. 24 Some dot states for $n = 3$ and $n = 4$. The total spins S of the states are indicated in brackets next to the lines that represent the level. The lines represent transitions that are allowed by the selection rules. Note that the transition between one of the three electron ground states (**b**) to the four electron ground state **d** is forbidden. The unusual behavior in the vicinity of the corresponding linear conductance peak is due to these five levels. It is necessary to include them all to find the main features of Fig. 23. Whether or not one includes further states in the calculations does not change the result qualitatively.

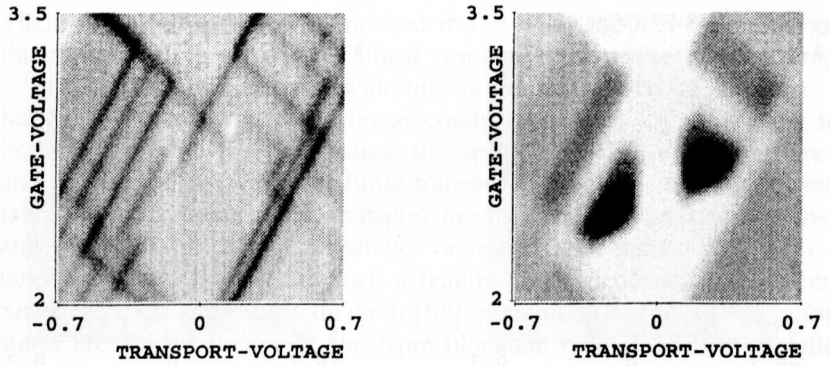

Fig. 25 Left: region around the transition between $n = 3$ and $n = 4$, magnified and with the energy of the $S = 3/2$ state **b** being slightly increased so that the degeneracy of the $n = 3$ ground states is lifted. At low but finite transport voltage the ground-state-to-ground-state transition is blocked because state **b** attracts almost all of the stationary occupation probability. Thus, negative differential conductances appear. Right: same region but now showing the population of the $n = 3$, $S = 3/2$ state (**b**) in dark. If the transport voltages are sufficient to occupy the $S = 3/2$ state it is easily populated but depopulation is difficult.

In order to simulate a rectangular dot, we enhance slightly the energy of the lowest $(n = 3; S = 3/2)$-state. Figure 25 shows (a) the differential conductance and (b) the stationary occupation probability of this state.

Now, the region of negative differential conductance is shifted in V by the excitation energy of the $(S = 3/2)$-state **b**. When the $(n = 3; S = 3/2)$-state starts to contribute, it attracts a large portion of the population at the expense of the $(n = 3; S = 1/2)$-ground state **a**. This suppresses the ground-state-to-ground-state transition. Only at even higher voltages the $(S = 3/2)$-state can again be depopulated and the line corresponding to transport involving the ground states is recovered. Striking features like this can be found in the greyscale representations of the experimental results [23, 29].

9 Summary and conclusions

We have investigated nonlinear transport through a small electron island, which is weakly coupled to reservoirs, taking into account Coulomb interaction between the electrons in the island, spin, magnetic field and non-equilibrium effects. The studies have been carried out in the parameter regime where charging and geometrical quantization effects coexist.

For different model Hamiltonians occupation probabilities, current-voltage characteristics and conductances versus gate-voltage at finite bias voltage were calculated using a rate equation.

Coupling to Boson modes leads to thermally induced intra-dot relaxation processes and to a suppression of the n lowest finestructure steps in the n-th Coulomb step of the I-V curve. Thsi was investigated in some detail for the charging model. The intra-dot relaxation provides thermal equilibrium only among the states with a given electron number. We demonstrated explicitly that the stationary non-equilibrium populations cannot be described by a Gibbs distribution. Consistent with previous investigations we find additional steps in the Coulomb staircase corresponding to transitions involving excited levels when the temperature is lower and the transport voltage higher than the excitation energies. We find pronounced asymmetries in the conductance peaks versus gate-voltage for asymmetric barriers, consistent with experimental findings.

By taking into account the quantum mechanical properties of the Coulombically interacting electrons including their spins, we demonstrated that spin selection rules can strongly influence the transport properties. This is important for semiconducting quantum dots with few electrons where electron correlations are expected to be important. The excitations of the n-electron system cannot be described by the occupation of single electron states, and the spins of all electrons are influenced when electron numbers are changed. The corresponding selection rules for transitions between states of different spin are very general and not restricted to our model. Spin conservation leads to a spin blockade effect and explains in a natural way various experimentally observed features which qualitatively cannot be explained by the charging model where excitations are treated as single particle excitations.

We proposed two qualitatively different types of spin blockades. They influence the heights of the linear conductance peaks and lead to negative nonlinear differential conductances. While the 'spin blockade of the first kind' is connected with spin-polarized states, the 'spin blockade of the second kind' is more general. It leads to qualitative changes even in linear transport, and is particularly important for 2D quantum dots.

The effects of an in-plane magnetic field were discussed. They explain recent experiments [23, 29, 34, 43]. The positions of the conductance peaks on the gate-voltage axis change with magnetic field. In quasi-1D quantum dots the sign of the shift at low field strength depends on the parity of the electron number. Level crossings lead to peak positions oscillating with magnetic field. The spin blockade phenomena disappear at sufficiently high magnetic fields when the spin polarized states become ground states.

All of the theoretically investigated features described above are consistent with recent experimental findings [23, 30–36]. In particular, the spin blockade effect is very likely to be the mechanism which causes negative differential conductances. Further experiments, in particular using 'slim quantum dots', are however necessary in order to clarify the quantitative aspects.

In experiments where the total spin of the electrons is not stable over times intervals long compared to the time between successive electron passages, the spin blockade is expected to disappear. By introducing an inhomogeneous magnetic field in the dot region (e.g. using type II superconductors on top of the structure or doping the sample with magnetic impurities) might also be a method to confirm unambiguously the importance of the spin blockade mechanism for quantum dot transport. Such experiments can in principle be carried out [69].

A Transition rates between the many-electron eigenstates of the isolated system

In this appendix, we show in detail how the transition rates (10) between the many-electron Fock-states of the correlated electrons in the dot are calculated using standard time-dependent perturbation theory in lowest order in the tunneling terms. The same method can be applied to determine the rates for the Anderson impurity (15, 16) and the charging model (29).

A.1 Time-dependent perturbation theory

If one can split up the Hamiltonian of the full system into two parts, $H = H_0 + H_p$, where the stationary Schrödinger-equation of the time-independent first term H_0

$$H_0 \mid \Psi_i^{(0)}\rangle = E_i^{(0)} \mid \Psi_i^{(0)}\rangle \tag{43}$$

can be solved exactly, yielding the eigenstates $\mid \Psi_i^{(0)}\rangle$ and the corresponding eigenenergies $E_i^{(0)}$, standard time-dependent perturbation theory gives the transition rates between eigenstates of H_0. In lowest order, one finds the transition rate

$$\gamma_{f,i} = \mid M_{f,i} \mid^2 \frac{2\pi}{\hbar}\delta(E_f^{(0)} - E_i^{(0)}) \tag{44}$$

with the matrix element

$$M_{f,i} = \langle \Psi_f^{(0)} \mid H_p \mid \Psi_i^{(0)}\rangle. \tag{45}$$

A.2 Effective transition rates between the many-electron dot states

Now, we specify the model to calculate the transition rates. We integrate over the lead states to find effective transition rates for the transitions between the eigenstates of the dot Hamiltonian.

First we have to remember that the state-vector used in the previous paragraph describes the whole system. In the unperturbed problem given by $H_0 = H_D + H_L + H_R + H_{Ph}$, the dot, the leads and the heat bath are completely decoupled and the Schrödinger-equation can be separated. Then, the total state-vector

$$\mid \Psi_i^{(0)}\rangle = \mid \Psi_{d_i}^{D}\rangle \mid \Psi_{l_i}^{L}\rangle \mid \Psi_{r_i}^{R}\rangle \mid \Psi_{Q_i}^{Ph}\rangle \tag{46}$$

is given by a product of the state-vector of the dot $|\Psi_{d_i}^{\mathrm{D}}\rangle$ and the ones describing the left/right lead $|\Psi_{l/r_i}^{\mathrm{L/R}}\rangle$ and the phonons $|\Psi_{Q_i}^{\mathrm{Ph}}\rangle$. The energies satisfying

$$H_{\mathrm{D}}|\Psi_{d_i}^{\mathrm{D}}\rangle = E_{d_i}^{\mathrm{D}}|\Psi_{d_i}^{\mathrm{D}}\rangle, \quad H_{\mathrm{L/R}}|\Psi_{l/r_i}^{\mathrm{L/R}}\rangle = E_{l/r_i}^{\mathrm{L/R}}|\Psi_{l/r_i}^{\mathrm{L/R}}\rangle,$$
$$H_{\mathrm{Ph}}|\Psi_{Q_i}^{\mathrm{Ph}}\rangle = E_{Q_i}^{\mathrm{Ph}}|\Psi_{Q_i}^{\mathrm{Ph}}\rangle, \tag{47}$$

are additive yielding

$$E_i^{(0)} = E_{d_i}^{(\mathrm{D})} + E_{l_i}^{(\mathrm{L})} + E_{r_i}^{(\mathrm{R})} + E_{Q_i}^{(\mathrm{Ph})}. \tag{48}$$

The small tunneling terms and the weak electron-phonon interaction in the Hamiltonian (8) are considered as the perturbation $H_{\mathrm{p}} = H_{\mathrm{L}}^{\mathrm{T}} + H_{\mathrm{R}}^{\mathrm{T}} + H_{\mathrm{ep}}$ allowing for transitions between the eigenstates of the isolated dot and the reservoirs. Since they lead to different transitions changing the state of different leads, we can treat the tunneling to and from the different leads and transitions involving no electron tunneling but phononic excitations separately. The tunneling terms can be written as a sum of two parts $H_{\mathrm{L/R}}^{\mathrm{T}} = H_{\mathrm{L/R}}^{\mathrm{T},-} + H_{\mathrm{L/R}}^{\mathrm{T},+}$ where the first,

$$H_{\mathrm{L/R}}^{\mathrm{T},-} = \sum_{k,m,\sigma} T_{k,m}^{\mathrm{L/R}} c_{\mathrm{L/R},k,\sigma}^{+} c_{m,\sigma} \tag{49}$$

describes tunneling of electrons out of the dot and the second part

$$H_{\mathrm{L/R}}^{\mathrm{T},+} = \sum_{k,m,\sigma} \left(T_{k,m}^{\mathrm{L/R}}\right)^{*} c_{m,\sigma}^{+} c_{\mathrm{L/R},k,\sigma} \tag{50}$$

corresponds to electrons entering the dot. These parts contain a sum over all the one-electron states in the leads and in the quantum dot.

The electron-phonon interaction terms can be written as a sum of two terms $H_{\mathrm{ep}} = H_{\mathrm{ep}}^{-} + H_{\mathrm{ep}}^{+}$ with

$$H_{\mathrm{ep}}^{\pm} = \sum_{q,m_1,m_2,\sigma} \sqrt{g(q,m_1,m_2)}\, c_{m_1,\sigma}^{+} c_{m_2,\sigma} a_q^{\pm} \tag{51}$$

where the first one describes the absorption of a phonon and the second part corresponds to the emission of a phonon. For simplicity, we assume the prefactor to be independent of all the parameters $g(q,m_1,m_2) \equiv g$.

A.2.1 Transitions with a reduction of the electron number in the dot

First, we treat the case of a transition in which an electron tunnels from the dot to the left/right lead. These transitions occur due to the first part of the tunneling Hamiltonian (49), which we insert in the expression for the transition matrix elements (45) and using (46), one gets the matrix elements

$$M_{f,i}^{\mathrm{L/R},-} = \sum_{m,\sigma} \sum_{k} T_{k,m}^{\mathrm{L/R}} D_{d_f,d_i;m,\sigma}^{-} A_{l/r_f,l/r_i;k,\sigma}^{\mathrm{L/R},-} B_{r/l_f,r/l_i}^{\mathrm{R/L}} C_{Q_f,Q_i}^{\mathrm{Ph}}, \tag{52}$$

where

$$D^{-}_{d_f,d_i;m,\sigma} = \langle \Psi^{\mathrm{D}}_{d_f} \mid c_{m,\sigma} \mid \Psi^{\mathrm{D}}_{d_i} \rangle\,, \quad A^{\mathrm{L/R},-}_{l/r_f,l/r_i;k,\sigma} = \langle \Psi^{\mathrm{L/R}}_{l/r_f} \mid c^{+}_{\mathrm{L/R},k,\sigma} \mid \Psi^{\mathrm{L/R}}_{l/r_i} \rangle$$
$$B^{\mathrm{R/L}}_{r/l_f,r/l_i} = \langle \Psi^{\mathrm{R/L}}_{r/l_f} \mid \Psi^{\mathrm{R/L}}_{r/l_i} \rangle\,, \quad C^{\mathrm{Ph}}_{Q_f,Q_i} = \langle \Psi^{\mathrm{Ph}}_{Q_f} \mid \Psi^{\mathrm{Ph}}_{Q_i} \rangle \tag{53}$$

are the terms which are connected to the different Hilbert spaces involved. The spin summation in (52) runs over the values $\sigma = \pm 1/2$ of the magnetic quantum number of the tunneling electron. Since the total spin and its z-component are conserved, $M_{d_f} - M_{d_i} = \pm 1/2$ and $\sigma = -\tilde{\sigma} := M_{d_f} - M_{d_i}$, and (52) can be simplified,

$$M^{\mathrm{L/R},-}_{f,i} = \sum_m \sum_k T^{\mathrm{L/R}}_{k,m}\, D^{-}_{d_f,d_i;m,-\tilde{\sigma}}\, A^{\mathrm{L/R},-}_{l/r_f,l/r_i;k,-\tilde{\sigma}}\, B^{\mathrm{R/L}}_{r/l_f,r/l_i}\, C^{\mathrm{Ph}}_{Q_f,Q_i}\,. \tag{54}$$

To obtain the effective rates for transitions between the dot states

$$\Gamma^{-}_{d_f,d_i} \equiv \left\langle \sum_{l_f,r_f,Q_f} \gamma^{-}_{f,i} \right\rangle_{\mathrm{th}(l_i,r_i,Q_i)}\,, \tag{55}$$

we sum over all the final states of the leads which are assumed to be coupled to reservoirs and the phonons. Matrix elements of the initial states of the leads and the phonons are evaluated assuming thermal equilibrium denoted by $\langle \cdots \rangle_{\mathrm{th}(l_i,r_i,Q_i)}$. Using (44) and (54) with (53), one gets

$$\begin{aligned}\Gamma^{-}_{d_f,d_i} = \frac{2\pi}{\hbar} \sum_{l_f,r_f,Q_f} \sum_{m,m'} \sum_{k,k'} \Big\langle & \Big(T^{\mathrm{L/R}}_{k,m}\Big)^{*} T^{\mathrm{L/R}}_{k',m'} \Big(D^{-}_{d_f,d_i;m,-\tilde{\sigma}}\Big)^{*} D^{-}_{d_f,d_i;m',-\tilde{\sigma}} \\ & \times \langle \Psi^{\mathrm{L/R}}_{l/r_i} \mid c_{\mathrm{L/R},k',-\tilde{\sigma}} \mid \Psi^{\mathrm{L/R}}_{l/r_f} \rangle \langle \Psi^{\mathrm{L/R}}_{l/r_f} \mid c^{+}_{\mathrm{L/R},k,-\tilde{\sigma}} \mid \Psi^{\mathrm{L/R}}_{l/r_i} \rangle \big) \\ & \times \langle \Psi^{\mathrm{R/L}}_{r/l_i} \mid \Psi^{\mathrm{R/L}}_{r/l_f} \rangle \langle \Psi^{\mathrm{R/L}}_{r/l_f} \mid \Psi^{\mathrm{R/L}}_{r/l_i} \rangle \langle \Psi^{\mathrm{Ph}}_{Q_i} \mid \Psi^{\mathrm{Ph}}_{Q_f} \rangle \langle \Psi^{\mathrm{Ph}}_{Q_f} \mid \Psi^{\mathrm{Ph}}_{Q_i} \rangle \Big\rangle_{\mathrm{th}(l_i,r_i,Q_i)} \\ & \times \delta(E^{(0)}_f - E^{(0)}_i).\end{aligned} \tag{56}$$

Since the set of orthonormal eigenfunctions $\mid \Psi^{\mathrm{L/R}}_{l/r_i} \rangle$ of the lead Hamiltonian $H_{\mathrm{L/R}}$ is complete, the sums over the final states of the leads give identity matrices and the two last factors in $\langle \cdots \rangle$ yield unity reflecting the fact that neither the right/left lead nor the phonons are affected by the process at all. Using the equilibrium expression

$$\langle \langle \Psi^{\mathrm{L/R}}_{l/r_i} \mid c_{\mathrm{L/R},k',-\tilde{\sigma}} c^{+}_{\mathrm{L/R},k,-\tilde{\sigma}} \mid \Psi^{\mathrm{L/R}}_{l/r_i} \rangle \rangle_{\mathrm{th}(l/r_i)} = [1 - f_{\mathrm{L/R}}(\varepsilon^{\mathrm{L/R}}_{k,-\tilde{\sigma}})] \delta_{k,k'}\,, \tag{57}$$

for the occupation number operator, where the Fermi-Dirac distribution function $f_{\mathrm{L/R}}(\varepsilon) = (\exp[\beta(\varepsilon - \mu_{\mathrm{L/R}})] + 1)^{-1}$ contains the temperature and the chemical potential of the reservoir, and using (48), which yields

$$E^{(0)}_f - E^{(0)}_i = E^{(\mathrm{D})}_{d_f} + \varepsilon^{\mathrm{L/R}}_{k,-\tilde{\sigma}} - E^{(\mathrm{D})}_{d_i} \tag{58}$$

in the argument of the Delta-function in (56) selects the value $k = k_E$ for the wave-vector in the left/right lead. We finally find

$$\Gamma^{-}_{d_f,d_i} = \frac{2\pi}{\hbar}\left|\sum_m T^{L/R}_{k_E,m} D^{-}_{d_f,d_i;m,-\tilde{\sigma}}\right|^2 \frac{\rho_{L/R}(E)}{2}\left[1 - f_{L/R}(E)\right] \tag{59}$$

with the energy of the tunneling electron $E = E^{(D)}_{d_i} - E^{(D)}_{d_f}$ and the density of states in the left/right lead $\rho_{L/R}$. A factor of $1/2$ arises because of the reduced density of states for a given electronic spin.

A.2.2 Transitions with an increase of the electron number in the dot

Now, we deal with an electron that tunnels from the left/right lead into the dot. Such transitions are due to the presence of the tunneling term (50). The calculation of the rates is analogous to the case of an electron tunneling out of the dot. Inserting (50) in (45) using (46), one gets the matrix elements for the increase of the electron number in the dot

$$M^{L/R,+}_{f,i} = \sum_m \sum_k \left(T^{L/R}_{k,m}\right)^* D^{+}_{d_f,d_i;m,\tilde{\sigma}} A^{L/R,+}_{l/r_f,l/r_i;k,\tilde{\sigma}} B^{R/L}_{r/l_f,r/l_i} C^{Ph}_{Q_f,Q_i} \tag{60}$$

with

$$D^{+}_{d_f,d_i;m,\sigma} = \langle \Psi^{D}_{d_f} \mid c^{+}_{m,\sigma} \mid \Psi^{D}_{d_i} \rangle \quad \text{and} \quad A^{L/R,+}_{l/r_f,l/r_i;k,\sigma} = \langle \Psi^{L/R}_{l/r_f} \mid c_{L/R,k,\sigma} \mid \Psi^{L/R}_{l/r_i} \rangle . \tag{61}$$

Again, we proceed by calculating the effective rates for transitions between the states of the dot and using now

$$\langle\langle \Psi^{L/R}_{l/r_i} \mid c^{+}_{L/R,k',\tilde{\sigma}} c_{L/R,k,\tilde{\sigma}} \mid \Psi^{L/R}_{l/r_i} \rangle\rangle_{\mathrm{th}(l/r_i)} = f_{L/R}(\varepsilon_k)\delta_{k,k'} , \tag{62}$$

one finds the result

$$\Gamma^{+}_{d_f,d_i} = \frac{2\pi}{\hbar}\left|\sum_m \left(T^{L/R}_{k_E,m}\right)^* D^{+}_{d_f,d_i;m,\tilde{\sigma}}\right|^2 \frac{\rho_{L/R}(E)}{2} f_{L/R}(E) . \tag{63}$$

A.2.3 Approximations

For the sake of simplicity, we neglect the dependence of the tunneling matrix elements on the electronic states and put

$$T^{L/R}_{k,m} \equiv T^{L/R} , \tag{64}$$

and introduce the abbreviations

$$t^{\mathrm{L/R}} = \frac{2\pi}{\hbar} \left| T^{\mathrm{L/R}} \right|^2 \rho_{\mathrm{L/R}}(E) , \tag{65}$$

neglecting the dependence of the density of states on the energy.

Thus, the effective transition rates between the eigenstates of the isolated dot take the simple form

$$\Gamma^{\pm}_{d_f,d_i} = \frac{t^{\mathrm{L/R}}}{2} \left| \sum_m D^{\pm}_{d_f,d_i;m,\pm\tilde{\sigma}} \right|^2 \left[\frac{1-(\pm 1)}{2} \pm f_{\mathrm{L/R}}(E) \right] . \tag{66}$$

Further, we extract the spin part of the state-vector describing the quantum dot, which is of very general nature and yields rich structure. From the consideration of the spin Hilbert space we find the squares of the vector coupling Clebsch-Gordan coefficients $\left| \langle S_{d_i}, M_{d_i}, \frac{1}{2}, \pm\frac{1}{2} \mid S_{d_f}, M_{d_f} \rangle_{\mathrm{CG}} \right|^2$ for the combination of the initial spin (S_{d_i}, M_{d_i}) with the spin of the tunneling electron $(1/2, \pm 1/2)$ to the spin of the final state (S_{d_f}, M_{d_f}) (for the values, see Table 2). To determine the exact matrix elements $D^{+/-}$, one has to go back to a microscopic model of the dot to calculate the orbital part of the many-electron wave-functions of the dot states, which will depend strongly on the details of the model. In principle, this can be done [58, 64], but in a first approach, we neglect this influence and approximate the dot matrix elements by

$$\left| \sum_m D^{+/-}_{d_f,d_i;m,\tilde{\sigma}} \right|^2 = \left| \left\langle S_{d_i}, M_{d_i}, \frac{1}{2}, +/-\tilde{\sigma} \mid S_{d_f}, M_{d_f} \right\rangle_{\mathrm{CG}} \right|^2 \delta_{n_f,n_i\pm 1} . \tag{67}$$

A.2.4 Transitions between dot states with the same electron number

The electron-phonon coupling leads to transitions between the dot states which do not change the electron number in the dot. Nevertheless, the state of the correlated electrons can be affected by the emission or absorption of a phonon.

We start with electron absorption processes. Inserting H^{-}_{ep} (51) in (45) using (46), one gets the matrix elements for this process

$$M^{\mathrm{Ph},-}_{f,i} = \sqrt{g} D^{\mathrm{Ph}}_{d_f,d_i} B^{\mathrm{L}}_{l_f,l_i} B^{\mathrm{R}}_{r_f,r_i} C^{\mathrm{Ph},-}_{Q_f,Q_i} \tag{68}$$

with

$$D^{\mathrm{Ph}}_{d_f,d_i} = \sum_{m_1,m_2,\sigma} \langle \Psi^{\mathrm{D}}_{d_f} \mid c^{+}_{m_1,\sigma} c_{m_2,\sigma} \mid \Psi^{\mathrm{D}}_{d_i} \rangle \text{ and } C^{\mathrm{Ph},-}_{Q_f,Q_i} = \sum_q \langle \Psi^{\mathrm{Ph}}_{Q_f} \mid a_q \mid \Psi^{\mathrm{Ph}}_{Q_i} \rangle . \tag{69}$$

The thermal average over the initial states of the phononic heat bath yields

$$\langle \Psi^{\mathrm{Ph}}_{Q_i} \mid a^{+}_q a_{q'} \mid \Psi^{\mathrm{Ph}}_{Q_i} \rangle_{\mathrm{th}(Q_i)} = n_{\mathrm{B}}(\hbar\omega_q)\delta_{q,q'} , \tag{70}$$

due to the bosonic nature of the phonons and one finds the result

$$\Gamma^{\mathrm{Ph}+}_{d_f,d_i} = \frac{2\pi}{\hbar} g \mid D^{\mathrm{Ph}}_{d_f,d_i} \mid^2 \rho_{\mathrm{L/R}}(E) n_{\mathrm{B}}(E) . \tag{71}$$

Inserting H^+_{ep} (51) in (45) using (46), one gets the matrix elements for the phonon emission process

$$M^{\mathrm{Ph},+}_{f,i} = \sqrt{g} D^{\mathrm{Ph}}_{d_f,d_i} B^{\mathrm{L}}_{l_f,l_i} B^{\mathrm{R}}_{r_f,r_i} C^{\mathrm{Ph},+}_{Q_f,Q_i} \text{ with } C^{\mathrm{Ph},-}_{Q_f,Q_i} = \sum_q \langle \Psi^{\mathrm{Ph}}_{Q_f} \mid a^+_q \mid \Psi^{\mathrm{Ph}}_{Q_i} \rangle . \tag{72}$$

Now using

$$\langle \Psi^{\mathrm{Ph}}_{Q_i} \mid a_q a^+_{q'} \mid \Psi^{\mathrm{Ph}}_{Q_i} \rangle_{\mathrm{th}(Q_i)} = [1 + n_{\mathrm{B}}(\hbar\omega_q)] \delta_{q,q'} , \tag{73}$$

one finds the result

$$\Gamma^{\mathrm{Ph}+}_{d_f,d_i} = \frac{2\pi}{\hbar} g \mid D^{\mathrm{Ph}}_{d_f,d_i} \mid^2 \rho_{\mathrm{L/R}}(E) [1 + n_{\mathrm{B}}(-E)] , \tag{74}$$

where the energy difference due to the phonon emission $E = -\hbar\omega_q$ is now negative. The rates (71) and (74) can be cast into one expression

$$\Gamma^{\mathrm{in}}_{d_f,d_i} = \frac{2\pi}{\hbar} g \mid D^{\mathrm{Ph}}_{d_f,d_i} \mid^2 \rho_{\mathrm{Ph}}(E) [n_{\mathrm{B}}(\mid E \mid) + \Theta(-E)] . \tag{75}$$

We neglect the dependence of the rate on the particular shape of the dot wavefunctions and the phononic density of states. For simplicity we set $r = (2\pi/\hbar) g \rho_{\mathrm{Ph}}$ and $\mid D \mid^2 = 1$.

The general case of the results (59), (63) and (75) is known in the literature as Fermi's Golden rule.

We thank Walter Pfaff with whom many aspects of transport through quantum dots within the charging model (Chapter 5) have been developed in an intensive collaboration.
We are indebted to Kristian Jauregui who carefully worked out the properties of interacting electrons in one dimension.
We thank R. Haug and J. Weis for discussions about experimental results on transport through quantum dots prior to publication. Further, we acknowledge discussions with many researchers in the field, in particular T. Brandes, C. Bruder, P. Hänggi, T. Heinzel, H. Heyszenau, G.-L. Ingold, J. Jefferson, U. Merkt, J.-L. Pichard, G. Platero, D. Pfannkuche, H. Schoeller, G. Schön, C. Tejedor, S. Ulloa and D. Wharam.
We thank the Physikalisch-Technische Bundesanstalt in Braunschweig, where a major part of this work was performed, for kind hospitality and support.
Financial support of the Deutsche Forschungsgemeinschaft via grant We 1124/4-1 and from the EU within the Science program, grant SCC*-CT90-0020 and within the HCM program, grants CHRX-CT93-0136 and ERB-CHBI-CT-94-1396, is gratefully acknowledged.

References

[1] Quantum Coherence in Mesoscopic Systems, B. Kramer (ed.), NATO ASI Series B **254**. Plenum Press, New York 1991
[2] B. Kramer, Festkörperprobleme/Advances in Solid State Physics **30** (1990) 53

[3] M.A. Kastner, Rev. Mod. Phys. **64** (1992) 849
[4] M.A. Kastner, Physics Today, p. 24, January 1993
[5] D.V. Averin, K. K. Likharev, J. Low Temp. Phys. **62** (1986) 345
[6] L.J. Geerligs, V.F. Anderegg, P.A.M. Holweg, J.E. Mooij, H. Pothier, D. Esteve, C. Urbina, M.H. Devoret, Phys. Rev. Lett. **64** (1990) 2691
[7] L.P. Kouwenhoven, A.T. Johnson, N.C. van der Vaart, A. van der Enden, C.J.P. Harmans, C.T. Foxon, Phys. Rev. Lett. **67** (1991) 1626
[8] L.P. Kouwenhoven, A.T. Johnson, N.C. van der Vaart, A. van der Enden, C.J.P. Harmans, C.T. Foxon, Zeitschr. Phys. **B 85** (1991) 381
[9] L.P. Kouwenhoven, PhD thesis, University of Delft 1992
[10] Special Issue on Single Charge Tunneling H. Grabert (ed.), Z. Phys. **B 85** (1991) 317–468
[11] M. H. Devoret et al., Bulletin du Bureau National de Métrologie **86** (1991) 7
[12] M. Devoret, D. Esteve, C. Urbina, Nature **360** (1992) 547
[13] C. Schönenberger, H. van Houten, H.C. Donkersloot, Europhys. Lett. **20** (1991) 249
[14] U. Merkt, J. Huser, M. Wagner, Phys. Rev. B **43** (1991) 7320
[15] P.A. Lee, Physica **B 189** (1993) 1
[16] Special Issue on Novel Physics in Low Dimensional Electron Systems T. Chakraborty (ed.), Physica B **212** (1995) 201–327
[17] Ch. Sikorski, U. Merkt, Phys. Rev. Lett. **62** (1989) 2164
[18] B. Meurer, D. Heitmann, K. Ploog, Phys. Rev. Lett. **68** (1992) 1371
[19] D. Heitmann, J.P. Kotthaus, Physics Today, p. 56, June 1993
[20] M. Wagner, A.V. Chpalik, U. Merkt, Phys. Rev. B **51**, 13817 (1995)
[21] W. Kohn, Phys. Rev. **123** (1961) 1242; A.O. Govorov, A.V. Chaplik, JETP Lett. **52** (1990) 31
[22] R.C. Ashoori, H.L. Stormer, J.S. Weiner, L.N. Pfeiffer, S.J. Pearton, K.W. Baldwin, K.W. West, Phys. Rev. Lett. **68** (1992) 3088
[23] J. Weis, R.J. Haug, K. v. Klitzing, K. Ploog, Phys. Rev. Lett. **71** (1993) 4019
[24] D. Weinmann, W. Häusler, W. Pfaff, B. Kramer, U. Weiss, Europhys. Lett. **26** (1994) 467
[25] T. Heinzel, S. Manus, D.A. Wharam, J.P. Kotthaus, G. Böhm, W. Klein, G. Tränkle, G. Weimann, Europhys. Lett. **26** (1994) 689
[26] U. Meirav, M.A. Kastner, S.J. Wind, Phys. Rev. Lett. **65** (1990) 771
[27] L.P. Kouwenhoven, N.C. van der Vaart, A.T. Johnson, W. Kool, C.J.P.M. Harmans, J.G. Williamson, A.A.M. Staring, C.T. Foxon, Z. Phys. **B 85** (1991) 367
[28] J.J. Palacios, L. Martin-Moreno, C. Tejedor, Europhys. Lett. **23** (1993) 495
[29] J. Weis, Ph. D. thesis, Stuttgart 1994
[30] J. Weis, R.J. Haug, K. v. Klitzing, K. Ploog, Phys. Rev. **B 46** (1992) 12837
[31] A.T. Johnson, L.P. Kouwenhoven, W. de Jong, N.C. van der Vaart, C.J.P.M. Harmans, C.T. Foxon, Phys. Rev. Lett. **69** (1992) 1592
[32] N.C. van der Vaart, A.T. Johnson, L.P. Kouwenhoven, D.J. Maas, W. de Jong, M.P. de Ruyter van Stevenick, A. van der Enden, C.J.P.M. Harmans, Physica **B 189** (1993) 99
[33] J. Weis, R.J. Haug, K. v. Klitzing, K. Ploog, Physica **B 189** (1993) 111
[34] J.T. Nicholls, J.E.F. Frost, M. Pepper, D.A. Ritchie, M.P. Grimshaw, G.A.C. Jones, Phys. Rev. **B 48** (1993) 8866
[35] E.B. Foxman, P.L. McEuen, U. Meirav, N.S. Wingreen, Y. Meir, P.A. Belk, N.R. Belk, M.A. Kastner, S.J. Wind, Phys. Rev. **B 47** (1993) 10020
[36] P.L. McEuen, N.S. Wingreen, E.B. Foxman, J. Kinaret, U. Meirav, M.A. Kastner, Y. Meir, S.J. Wind, Physica **B 189** (1993) 70
[37] W. Pfaff, D. Weinmann, W. Häusler, B. Kramer, U. Weiss, Z. Phys. **B 96** (1994) 201
[38] D. Weinmann, W. Häusler, B. Kramer, Phys. Rev. Lett. **74** (1995) 984
[39] W. Häusler, K. Jauregui, D. Weinmann, T. Brandes, B. Kramer, Physica **B 194–196** (1994) 1325
[40] D. Weinmann, W. Häusler, K. Jauregui, B. Kramer, in 'Quantum Dynamics of Submicron Structures', H.A. Cerdeira, B. Kramer, G. Schön (eds.), NATO ASI Series E–Vol. 291 (1995) 297
[41] W. Häusler, K. Jauregui, D. Weinmann, T. Brandes, B. Kramer, Physica **B 194–196** (1994) 1325
[42] J.M. Kinaret, Y. Meir, N.S. Wingreen, P.A. Lee, X.-G. Wen, Phys. Rev. **B 46** (1992) 4681
[43] J. Weis, R. Haug, K. v. Klitzing, K. Ploog, Surf. Sci. **305** (1994) 664
[44] M.H. Cohen, L.M. Falicov, J.C. Phillips, Phys. Rev. Lett. **8** (1962) 316
[45] R.E. Prange, Phys. Rev. **131** (1963) 1083
[46] D. Weinmann, Ph. D. thesis, Universität Hamburg 1994, ISBN 3-89429-542-2
[47] G.D. Mahan, Many-Particle Physics, 2nd ed. Plenum, New York 1990
[48] U. Weiss, Quantum Dissipative Systems. World Scientific, Singapore 1993
[49] D.V. Averin, G. Schön in Ref. [1], p. 531
[50] Y. Meir, N.S. Wingreen, P.A. Lee, Phys. Rev. Lett. **66** (1991) 3048
[51] H. Schoeller, G. Schön, Phys. Rev. **B50** (1994) 18436

[52] C.W.J. Beenakker, Phys. Rev. **B 44** (1991) 1646
[53] D.V. Averin, A.N. Korotkov, Journ. of Low Temp. Phys. **80** (1990) 173
[54] D.V. Averin, A.N. Korotkov, K.K. Likharev, Phys. Rev. **B 44** (1991) 6199
[55] T. Brandes, W. Häusler, K. Jauregui, B. Kramer, D. Weinmann, Physica **B 189** (1993) 16
[56] W. Häusler, B. Kramer, J. Mašek, Z. Phys. **B 85** (1991) 435
[57] W. Häusler, B. Kramer, Phys. Rev. **B 47** (1993) 16353
[58] K. Jauregui, W. Häusler, B. Kramer, Europhys. Lett. **24** (1993) 581
[59] W. Häusler, Festkörperprobleme/Adv. in Solid State Physics **34**, R. Helbig (ed.), Vieweg, Braunschweig 1994, p. 171
[60] D.V. Averin, A.A. Odintsov, Phys. Lett. **A 140** (1989) 251
[61] D.V. Averin, Yu.V. Nazarov, in: Single Charge Tunneling, H. Grabert, M.H. Devoret (eds.). Plenum, New York 1991
[62] P.W. Anderson, Phys. Rev. **124** (1961) 41
[63] V.I. Fal'ko, Europhys. Lett. **8** (1989) 785
[64] K. Jauregui, W. Häusler, D. Weinmann, B. Kramer, Phys. Rev. **B 53**, R1713 (1996); K. Jauregui, Ph. D. thesis, Hamburg 1995, ISBN 3-89429-665-8
[65] D. Pfannkuche, S.E. Ulloa, Phys. Rev. Lett. **74** (1995) 1194
[66] N.C. van der Vaart, M.P. de Ruyter van Steveninck, L.P. Kouwenhoven, A.T. Johnson, Y.V. Nazarov, C.J.P.M. Harmans, C.T. Foxon, Phys. Rev. Lett. **73** (1994) 320
[67] F. Stern, Phys. Rev. Lett. **21** (1968) 1687
[68] E. Lieb, D. Mattis, Phys. Rev. **125** (1962) 164
[69] D.A. Wharam, private communication 1994